



1           **Enhancing Winter Climate Simulations of the Great Lakes:**  
2           **Insights from a New Coupled Lake-Ice-Atmosphere (CLIAv1)**  
3           **Model on the Importance of Integrating 3D Hydrodynamics with**  
4           **a Regional Climate Model**

5   Pengfei Xue<sup>1,2,3</sup>, Chenfu Huang<sup>2</sup>, Yafang Zhong<sup>4</sup>, Michael Notaro<sup>4</sup>, Miraj B. Kayastha<sup>1</sup>, Xing  
6   Zhou<sup>1</sup>, Chuyan Zhao<sup>2</sup>, Christa Peters-Lidard<sup>5</sup>, Carlos Cruz<sup>5</sup>, Eric Kemp<sup>5</sup>

7

8   <sup>1</sup> Department of Civil, Environmental and Geospatial Engineering, Michigan Technological  
9   University, Houghton, MI, USA

10   <sup>2</sup> Great Lakes Research Center, Michigan Technological University, Houghton, MI, USA

11   <sup>3</sup> Environmental Science Division, Argonne National Laboratory, Lemont, IL, USA

12   <sup>4</sup> Nelson Institute Center for Climatic Research, University of Wisconsin-Madison, Madison,  
13   WI, USA

14   <sup>5</sup> National Aeronautics and Space Administration Goddard Space Flight Center, Greenbelt, MD,  
15   USA

16

17

18   *Correspondence to:* Pengfei Xue, pexue@mtu.edu

19



## 20 **Abstract**

21 The Laurentian Great Lakes significantly influence the climate of the Midwest and Northeast  
22 United States, due to their vast thermal inertia, moisture source potential, and unique heat and  
23 moisture flux dynamics. This study presents a newly developed coupled lake-ice-atmosphere  
24 (CLIAv1) modeling system for the Great Lakes by coupling the National Aeronautics and  
25 Space Administration (NASA)-Unified Weather Research and Forecasting (NU-WRF) regional  
26 climate model (RCM) with the three-dimensional (3D) Finite Volume Community Ocean  
27 Model (FVCOM) and investigates the impact of coupled dynamics on simulating the Great  
28 Lakes' winter climate. By integrating 3D lake hydrodynamics, CLIAv1 addresses the  
29 limitations of traditional one-dimensional (1D) lake and demonstrates superior performance in  
30 reproducing observed LSTs, ice cover distribution, and the vertical thermal structure of the  
31 Great Lakes compared to the NU-WRF model coupled with the default 1D Lake Ice Snow and  
32 Sediment Simulator (LISSS). CLIAv1 also enhances simulation of over-lake atmospheric  
33 conditions, including air temperature, wind speed, and sensible and latent heat fluxes,  
34 underscoring the importance of resolving complex lake dynamics for reliable climate  
35 projections. More importantly, this study addresses the crucial question about what are the key  
36 processes influencing lake thermal structure and ice cover that are missed by 1D lake models  
37 but effectively captured by 3D lake models. Through process-oriented numerical experiments,  
38 we identify key 3D hydrodynamic processes—ice transport, heat advection, and shear  
39 production in turbulence—that explain the superiority of 3D lake models over 1D lake models,  
40 particularly in cold season performance and lake-atmosphere interactions. Properly resolving  
41 these processes using 3D hydrodynamic model is crucial for successfully simulating the lake-  
42 ice-atmosphere coupled Great Lakes winter system. This research underscores the necessity of  
43 incorporating 3D hydrodynamic models in RCMs to improve our predictive understanding of  
44 the Great Lakes' response to climate change. The findings advocate for a shift towards high-  
45 resolution, physics-based modeling approaches to ensure accurate future climate and  
46 limnological projections for large freshwater systems.

47



## 48 1 Introduction

49 The Laurentian Great Lakes, with a surface area of 246,000 km<sup>2</sup>, represent Earth's largest  
50 surface freshwater resources, containing 21% of the world's surface freshwater and 84% of  
51 North America's surface freshwater (Botts and Krushelnicki, 1987; EPA, 2014; Notaro et al.,  
52 2015; Xue et al., 2022). Over 55 million people live within the Great Lakes' megaregion  
53 (Todorovich, 2009; Sharma et al., 2018). The lakes support the United States' and Canadian  
54 economies by impacting drinking water supply, shipping, fishing, power production,  
55 transportation, manufacturing, wastewater treatment, agriculture, and recreation (Vaccaro and  
56 Read, 2011). The Great Lakes' support of these vital industries sustains approximately 1.3  
57 million jobs and \$82 billion in annual wages (Rau et al., 2020). As an invaluable resource to  
58 wildlife and society, the ecologically diverse Great Lakes Basin is home to over 3,500 animal  
59 and plant species, including over 170 fish species (Botts and Krushelnicki, 1987; Crossman and  
60 Cudmore, 1998; EPA, 2014). The basin's wetlands serve as spawning and nesting habitat,  
61 reduce erosion, and protect water quality (Notaro et al., 2015).

62 The Great Lakes are critically important in terms of their impacts on the climate of the Midwest  
63 and Northeast United States and southern Ontario, Canada. The regional climate is highly  
64 sensitive to the Great Lakes due to the lakes' vast thermal inertia, potential source of moisture  
65 to the overlying atmosphere, and contrasts in heat, moisture, roughness, and albedo compared  
66 to surrounding land (Changnon and Jones, 1972; Scott and Huff, 1996; Chuang and Sousounis,  
67 2003; Notaro et al., 2013a; Briley et al., 2021; Wang et al., 2022). During late autumn through  
68 winter, when cold, dry continental air masses from Canada pass over the relatively mild Great  
69 Lakes, the air masses are destabilized and moistened, leading to enhanced cloud cover and  
70 precipitation downwind of the lakes (Niziol et al., 1995; Ballentine et al., 1998; Kristovich and  
71 Laird, 1998; Notaro et al., 2013b; Shi and Xue, 2019). During the broader unstable lake season,  
72 which spans from September to March and is characterized by amplified lake-effect cloud  
73 cover and precipitation due to lake surface temperatures typically exceeding overlying air  
74 temperatures, lake-effect snowfall typically peaks during December-January, and lake ice cover  
75 is most extensive during February-March (Assel, 1990; Niziol et al., 1995; Kristovich and  
76 Laird, 1998; Lam and Schertzer, 1999; Notaro et al., 2013b). The establishment of extensive  
77 lake ice cover usually by mid-late winter dampens over-lake turbulent fluxes of heat and



78 moisture, subsequently reducing resulting lake-effect precipitation (Brown and Duguay, 2010;  
79 Notaro et al., 2021). Specifically, increasing lake ice cover leads to a linear reduction in latent  
80 heat fluxes and nonlinear reduction in sensible heat fluxes (Gerbush et al., 2008). When  
81 relatively cool (warm) air masses pass over the Great Lakes during winter (summer), the  
82 relatively warm (cool) lake surface reduces (enhances) atmospheric stability and increases  
83 (decreases) deep convection, cloud cover, and precipitation (Scott and Huff, 1996; Holman et  
84 al., 2012; Bennington et al., 2014). The lakes' relatively low roughness compared to the  
85 surrounding land leads to strengthened over-lake wind speeds and potential shoreline  
86 convergence in support of enhanced lake-effect precipitation. Due to the lakes' large thermal  
87 inertia and resulting seasonal evolution in lake-air temperature contrast, the Great Lakes  
88 typically strengthen wintertime cyclones and summer anticyclones and weaken summertime  
89 cyclones and wintertime anticyclones (Notaro et al., 2013a). The basin is a preferred zone of  
90 wintertime cyclogenesis due to the relative warmth of the lake surfaces and consequential  
91 enhancement in low-level convergence (Petterssen and Calabrese, 1959; Colucci, 1976;  
92 Eichenlaub, 1978).

93 Given the aforementioned substantial influence of the Great Lakes on regional climate, their  
94 representation and evaluation in both global and regional climate models have been the focus of  
95 several studies in the past decade. There is a wide spectrum among climate models regarding  
96 the treatment of large lakes. Due to their coarse spatial resolution, most global climate models  
97 (GCMs), including those from various phases of the Coupled Model Intercomparison Project  
98 (CMIP), either omit the Great Lakes entirely or offer a crude representation using wet soil,  
99 wetlands, ocean grid cells, or 1D lake models (Briley et al., 2021; Minallah and Steiner, 2021).

100 Among regional climate models (RCMs) without lake models, many apply a rudimentary  
101 approach to estimate lake surface temperatures (LSTs) by extrapolating the closest ocean grid  
102 cell's sea-surface temperatures (SSTs), likely from Hudson Bay or the North Atlantic Ocean,  
103 from the initial and lateral boundary conditions datasets to the lake grid cell, potentially  
104 inducing vast biases and intra-lake discontinuities in LST and ice cover (Gao et al., 2012;  
105 Mallard et al., 2015; Spero et al., 2016; Xiao et al., 2016; Hanrahan et al., 2021). This approach  
106 is the default treatment of LSTs in the Weather Research and Forecasting (WRF) model  
107 (Hanrahan et al., 2021; Wang et al., 2022). Alternatively, the WRF Preprocessing System can



108 designate time-averaged 2-m air temperatures to the underlying lake surfaces to provide  
109 estimated lower boundary conditions of LST based on the user-specified time window for  
110 temporal averaging and time lag for addressing thermal inertia (Wang et al., 2012; Mallard et  
111 al., 2015; Hanrahan et al., 2021; Wang et al., 2022). However, this approach still produces  
112 unrealistic LSTs and ice cover as the lakes cannot achieve equilibrium with the overlying  
113 atmosphere due to the lack of interactive lake-atmosphere feedbacks (Bullock et al., 2014;  
114 Spero et al., 2016).

115 For those GCMs and RCMs that aim to incorporate coupled lake-atmosphere interactions, most  
116 apply 1D lake models (Perroud et al., 2009; Martynov et al., 2010; Stepanenko et al., 2010;  
117 Subin et al., 2012). Those include 2-layer bulk models founded in similarity theory such as the  
118 Freshwater Lake (FLake) model (Mironov et al., 2010), thermal diffusion models which  
119 parameterize eddy diffusivity such as the Minnesota Lake Water Quality Management Model  
120 (MINLAKE, Riley and Stefan, 1988) and the Hostetler model (Hostetler and Bartlein, 1990),  
121 Lagrangian turbulence models such as the Dynamics Reservoir Simulation Model (DYRSM,  
122 Yeates and Imberger, 2003), and  $k-\epsilon$  turbulence closure models with horizontally averaged  
123 velocity such as LAKE (Stepanenko and Lykossov, 2005; Stepanenko et al., 2011) and Simstrat  
124 (Goudsmit et al., 2002). Each of these different categories of 1D lake models has its own  
125 advantages and disadvantages (Perroud et al., 2009; Martynov et al., 2010; Stepanenko et al.,  
126 2010; Subin et al., 2012). As demonstrated in these studies, the deficiencies include struggles  
127 with simulating seasonal stratification in FLake, insufficient mixing for deep lakes in the  
128 Hostetler model, and excessive mixing for shallow lakes in the computationally expensive  
129 turbulence models.

130 Multiple modeling studies have assessed the performance of coupling RCMs to 1D lake models  
131 in the Great Lakes region. While this coupling permits the representation of key lake-  
132 atmosphere interactions and the heterogeneous spatiotemporal patterns of LSTs and lake ice  
133 cover, 1D lake models typically perform poorly at reproducing the lake thermal structure and  
134 seasonal ice evolution of large, deep lakes, such as Lake Superior, due to the overly simplified  
135 hydrodynamic processes. Common biases in 1D lake models include an anomalously early  
136 timing of both spring-summer stratification and autumn turnover, with positive biases in  
137 summer LST and negative biases in winter LST (Bennington et al., 2014; Mallard et al., 2014).



138 The International Centre for Theoretical Physics (ICTP) Regional Climate Model version 4  
139 (RegCM4), coupled to the 1D Hostetler lake model, yields a prolonged lake ice season with  
140 excessive ice cover due to the neglect of horizontal heat advection within the lakes (Notaro et  
141 al., 2013b). The coupling of a thermal diffusion lake model, the Lake, Ice, Snow and Sediment  
142 Simulator (LISSS, Subin et al., 2012) to the WRF model (available starting with version 3.6 of  
143 WRF) results in an early warm-up and overly rapid cool-down in the seasonal evolution of  
144 LSTs for deep lakes, along with an early onset of lake ice cover in support of its excessive  
145 abundance (Xiao et al., 2016). Mallard et al. (2014) found that WRF, coupled to FLake,  
146 produced the best performance for Lake Erie (the smallest and shallowest Great Lake) and the  
147 worst performance for Lake Superior (the largest and deepest Great Lake) among the Great  
148 Lakes in terms of simulated LST and ice cover biases. Often, modelers aim to reduce biases in  
149 the simulated vertical temperature profile of deep lakes in 1D models by artificially enhancing  
150 the vertical eddy diffusivity to crudely compensate for the absence of a dynamic circulation and  
151 vertical mixing processes (Subin et al., 2012; Bennington et al., 2014; Lofgren, 2014; Gu et al.,  
152 2015; Mallard et al., 2015), although such a non-physics based approach may only yield limited  
153 benefits to minimizing these biases (Xiao et al., 2016). The lack of fully resolved lake  
154 hydrodynamics in models, including dynamic 3D lake circulation, upwelling and downwelling,  
155 thermal bar formation, explicit horizontal mixing, and ice motion, along with overly simplified  
156 stratification processes, unrealistic treatment of eddy diffusivity, and the assumption of  
157 instantaneous mixing of thermal instabilities (Song et al., 2004; Martynov et al., 2010, 2012;  
158 Stepanenko et al., 2010; Bennington et al., 2014; Gu et al., 2015; Mallard et al., 2015; Sharma  
159 et al., 2018; Sun et al., 2020; Notaro et al., 2021; Hutson et al., 2024) has been the main  
160 obstacle in further improving climate simulations for the Great Lakes Basin.

161 In recent years, a limited number of Great Lakes studies have aimed to enhance the  
162 representation of three-dimensional (3D) lake hydrodynamical processes and reduce the  
163 substantial biases in LST and ice cover associated with 1D lake models by coupling RCMs with  
164 3D hydrodynamic models (Xue et al., 2017, 2022; Sun et al., 2020; Kayastha et al., 2023).  
165 These studies have responded to the urgent call for continued progress in coupling high-  
166 resolution RCMs with 3D lake models that address the complex processes and features of large,  
167 deep lakes, as highlighted in previous research (Martynov et al., 2010; Bennington et al., 2014;  
168 Briley et al., 2021; Notaro et al., 2021). Xue et al. (2017) developed a two-way coupled 3D



169 lake-ice-climate modeling system, known as the Great Lakes-Atmosphere Regional Model  
170 (GLARM), by coupling RegCM4 with a 3D unstructured-grid hydrodynamic model, the Finite  
171 Volume Community Ocean Model (FVCOM, Chen et al., 2012). The resulting coupled 3D  
172 modeling system exhibited notable skill in reproducing the mean, variability, and trends in  
173 regional climate across the Great Lakes Basin and the physical characteristics of the Great  
174 Lakes, including their thermal structure and ice cover, significantly improving upon previous  
175 RCM experiments coupled with 1D lake models. The updated version, GLARM-V2, has been  
176 utilized to generate future climatic and limnological projections for the Great Lakes region  
177 (Xue et al., 2022). Similarly, Sun et al. (2020) developed a lake-atmosphere-hydrology  
178 modeling system by coupling the Climate-WRF (CWRF) model with 3D FVCOM and  
179 compared its performance against CWRF coupled with the 1D LISSS. They found that the  
180 former configuration outperformed the latter in simulating LST, ice cover, and the vertical  
181 thermal structure in the Great Lakes. Kayastha et al. (2023) developed and validated the WRF-  
182 FVCOM Two-way Coupling (WF2C) model, showing WF2C improved upon past 1D lake  
183 model-based studies by significantly reducing the simulated summer LST bias, and revealing  
184 how coupled lake-atmosphere dynamics can influence summer LST by modifying surface heat  
185 fluxes through impacts on meteorological state variables. These studies underscore the  
186 advantages of coupling an RCM with a 3D lake hydrodynamic model for accurately depicting  
187 lake physical processes and lake-atmosphere feedbacks in the Great Lakes Basin. However,  
188 there is a notable absence of research dedicated to identifying the fundamental processes  
189 resolved in 3D lake models that contribute to these improvements, which is important to  
190 optimize effort allocation in future model development and improve our predictive  
191 understanding of the system. This knowledge gap is particularly significant for the Great Lakes  
192 during the winter seasons.

193 This paper attempts to address this knowledge gap, by developing a new coupled lake-ice-  
194 atmosphere (CLIA version 1 or CLIAv1) modeling system for the Great Lakes by coupling the  
195 National Aeronautics and Space Administration (NASA)-Unified Weather Research and  
196 Forecasting (NU-WRF) regional climate model (RCM) with the three-dimensional (3D) Finite  
197 Volume Community Ocean Model (FVCOM). Note that CLIAv1 is hereinafter referred to as  
198 NU-WRF/FVCOM for the sake of particular attention given to comparing NU-WRF's  
199 performance during the cold season when two-way coupled with 3D FVCOM (NU-



200 WRF/FVCOM) versus 1D LISSS (NU-WRF/LISSS). After a thorough validation of the  
201 coupled model, we conduct a series of process-oriented numerical experiments to identify the  
202 most important hydrodynamic processes that contribute to the superiority of the 3D lake model  
203 over the 1D lake model in enhancing lake-atmosphere coupling for the Great Lakes.

## 204 **2 Model, Data, and Numerical Experiment Design**

### 205 **2.1 Atmosphere Model**

206 NU-WRF is an observation-driven integrated regional modeling system, developed at NASA's  
207 Goddard Space Flight Center (GSFC), that resolves chemistry, aerosol, cloud, precipitation and  
208 land processes at satellite-resolvable scales (roughly 1–25 km) to improve the continuity  
209 between microscale, mesoscale and synoptic processes. Developed as a superset of the  
210 community WRF, NU-WRF unifies the NCAR - Advanced Research version of WRF model  
211 (WRF-ARW) with the GSFC Land Information System (LIS, Kumar et al., 2006; Peters-Lidard  
212 et al., 2007, 2015), the Goddard Chemistry Aerosol Radiation and Transport (GOCART) model  
213 (Chin et al., 2000), the Goddard radiation and microphysics schemes (Shi et al., 2014), and the  
214 Goddard Satellite Data Simulator Unit (G-SDU, Matsui et al., 2013, 2014). NU-WRF  
215 simulations here utilize the Noah Land Surface Model, which simulates soil moisture and  
216 temperature, skin temperature, snowpack depth and the energy flux and water flux terms of the  
217 surface energy balance and surface water balance (Mitchell, 2005). Currently, by default, the  
218 two-way lake-atmosphere interactions in NU-WRF are represented using the embedded 1D  
219 LISSS (Subin et al., 2012) from the Community Land Model version 4.5 (Oleson et al., 2013)  
220 with modifications by Gu et al. (2015).

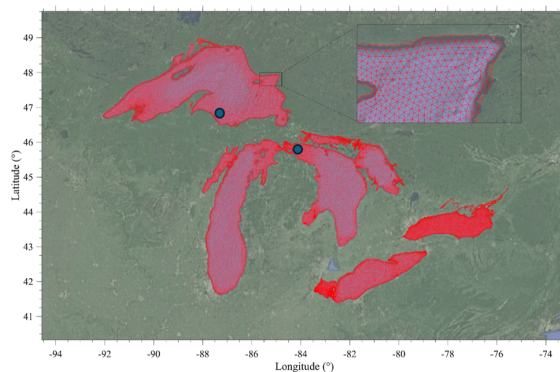
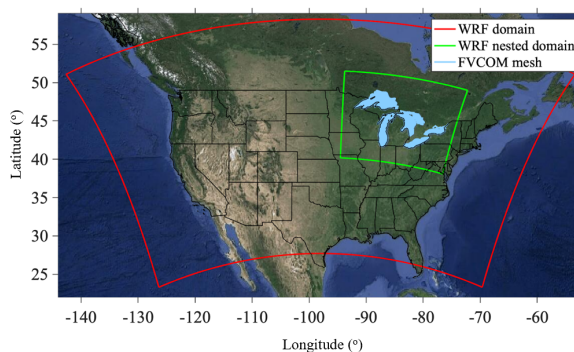
221 Notaro et al. (2021) conducted 20 simulations to identify the regionally optimal NU-WRF  
222 configuration and schemes for the cold season period of November 2014-March 2015 in the  
223 Great Lakes region. The best model configuration was referred to as the “Morrison  
224 combination” and is used in this study. The “Morrison combination” includes Morrison  
225 microphysics (Morrison et al., 2009), Rapid Radiative Transfer Model (RRTM, Mlawer et al.,  
226 1997) longwave radiation physics, Community Atmosphere Model (CAM, Collins et al., 2004)  
227 shortwave radiation physics, Mellor-Yamada-Nakanishi-Niino Level 2.5 (MYNN2.5,  
228 Nakanishi and Niino, 2006, 2009) planetary boundary layer physics, and Mellor-Yamada-





229 Nakanishi-Niino (MYNN, Nakanish, 2001) surface layer schemes. The improved simulations  
230 of air temperature and surface insolation using the Morrison combination primarily benefits  
231 from the Community Atmosphere Model's shortwave radiation scheme (Notaro et al., 2021).  
232 The Morrison combination is essentially the WRF configuration determined by Mooney et al.  
233 (2013) to produce the best simulated wintertime temperature simulation over Europe, who  
234 found that winter air temperatures are highly sensitive to the choice of radiation physics.

235 The NU-WRF one-way nested configuration consists of an outer domain with 15-km grid  
236 spacing for the majority of North America and an inner domain with 3-km grid spacing for the  
237 Great Lakes region (Fig. 1), with the atmospheric vertical resolution assigned to 61 levels. The  
238 initial and lateral boundary conditions are provided by the Global Data Assimilation System 0-  
239 hour analysis. The cumulus parameterization option used for the outer domain is the Kain-  
240 Fritsch scheme (Kain and Fritsch, 1990; Kain, 2004) with resolved, unparameterized  
241 convection in the inner domain.



242



243 **Figure 1.** NU-WRF nested domains (upper panel) and unstructured mesh used in FVCOM to represent  
244 the Great Lakes in FVCOM (lower panel). The two dots denote the locations of Granite Island (87.4°W,  
245 46.7°N) on Lake Superior and Spectacle Reef (84.1°W, 45.7°N) on Lake Huron.

## 246 **2.2 Hydrodynamic Model**

247 The hydrodynamic model, FVCOM, is a free-surface, primitive equation hydrodynamic model  
248 that solves the momentum, continuity, temperature, salinity, and density equations and is closed  
249 physically and mathematically using turbulence closure submodels (Chen et al., 2012).

250 Numerically, FVCOM employs the finite-volume method over an unstructured triangular grid  
251 and vertical sigma layers, optimizing flexibility and accuracy for complex terrains. The grid  
252 resolution adjusts from 1–2 km near coasts to resolve coastal geometry complexity, to 2–4 km  
253 offshore to improve computational efficiency (Fig. 1), with the model comprising 35,000 grid  
254 cells and 40 sigma layers. Vertical mixing processes are modeled using the Mellor–Yamada  
255 level-2.5 (MY25) turbulence closure model (Mellor and Yamada, 1982), while horizontal  
256 diffusivity is derived from velocity shear and grid resolution through the Smagorinsky (1963)  
257 formulation.

258 FVCOM also includes an unstructured-grid, finite-volume version of the Los Alamos  
259 Community Ice Code (CICE), which describes ice thickness distribution in time and space.  
260 CICE includes a thermodynamic model to compute local growth rates of snow and ice due to  
261 vertical conductive, radiative, and turbulent fluxes. It also features an ice dynamics model to  
262 simulate the ice pack velocity due to wind and ice-water stress, Coriolis effects, sea surface  
263 slope, and internal stress, estimated with elastic–viscous–plastic rheology (Hunke and  
264 Dukowicz, 1997). The transport model in CICE calculates the advective process of the areal  
265 concentration, ice volumes, and other state variables. The ridging parameterization in CICE  
266 addresses mechanical redistribution, which transfers ice among thickness categories (Hunke et  
267 al., 2010).

268 In contrast, the default 1D lake model, LISSS, embedded in NU-WRF solves the 1D thermal  
269 diffusion equation (i.e. lake thermal dynamics only) by segmenting the vertical stratification of  
270 the lake into multiple distinct levels that include: snow (applicable when the snow's thickness  
271 surpasses a specified minimum value); the combined section of lake water and ice, collectively



272 identified as the "lake body"; and the bottom layers consisting of sediment, soil, and bedrock  
273 (collectively termed "sediment" unless specified differently). This structured division allows for  
274 simulating thermal dynamics within each segment, facilitating a prediction of temperature  
275 distribution and variations across the lake's depth (Subin et al., 2012).

### 276 **3 Two-way Coupling of NU-WRF/FVCOM**

277 The development of interactively coupled model systems [see review by Giorgi and Gutowski  
278 Jr. (2015)] emerged quickly in the late 2000s driven by rapid technological advancement and  
279 the increase in computational capability. Model coupling is essential to multi-physics  
280 simulations representing various components of the Earth system. Over the past two decades,  
281 several coupling technologies for earth system modeling have been developed. Examples  
282 include the Earth System Modeling Framework (ESMF), the Model Coupling Toolkit (MCT),  
283 and the OASIS-MCT coupler, which is the latest version of the OASIS3 coupler interfaced with  
284 the Model Coupling Toolkit (MCT) that offers a fully parallel implementation of coupling field  
285 regridding and exchange (Valcke et al., 2012; Craig et al., 2017). Although coupling  
286 implementations can follow different approaches, their applications in geophysical simulations  
287 typically carry out several key functions, including interpolating and transferring the coupling  
288 fields between different model grids, managing data transfer between constitutive models at a  
289 desired coupling frequency, and coordinating the execution of the constituent models in a  
290 parallel computational environment (Valcke et al., 2012). In general, coupling data must be  
291 interpolated and transferred between the constituent models under several constraints, such as  
292 conservation of physical properties, numerical stability, consistency with physical processes,  
293 and computational efficiency.

294 In the study, NU-WRF and FVCOM are run simultaneously, exchanging information  
295 bidirectionally at 1-hour intervals through the OASIS3-MCT coupler. FVCOM dynamically  
296 calculates the LST and ice cover, providing these as overlake surface boundary conditions to  
297 NU-WRF. Meanwhile, NU-WRF calculates and supplies the atmospheric forcings required by  
298 FVCOM, including surface air temperature, surface air pressure, relative and specific humidity,  
299 total cloud cover, surface winds, and downward shortwave and longwave radiation.



### 300 3.1 Data for Model Validation

301 The average daily LST, obtained from composite images taken by the Advanced Very High  
302 Resolution Radiometer, is sourced from version 2 of the Great Lakes Surface Environmental  
303 Analysis (GLSEA) LST Dataset, developed by the National Oceanic and Atmospheric  
304 Administration's (NOAA) Great Lakes Environmental Research Laboratory (GLERL). A  
305 comprehensive evaluation carried out by Schwab et al. (1999) shows that LST measurements  
306 from GLSEA and the buoy-based LSTs had an average discrepancy of less than 0.5°C across  
307 all buoys, with a root-mean-square difference (RMSD) between 1.10°C and 1.76°C. The Great  
308 Lakes Ice Cover Dataset, compiled by GLERL, has also been added to the GLSEA product.  
309 The dataset incorporates daily average ice cover data across the lakes, which draws from ice  
310 products produced by the United States National Ice Center and the Canadian Ice Service, and  
311 is detailed in studies by Assel et al. (2002, 2013), Assel (2005), and Wang et al. (2012).

312 In-situ lake thermistor measurements for vertical lake thermal structure were obtained from  
313 Spectacle Reef on Lake Huron (Fig. 1). Measurements for over-lake atmospheric variables,  
314 including air temperature, wind velocity, downward shortwave radiation, and sensible and  
315 latent heat fluxes, were obtained from Granite Island on Lake Superior and Spectacle Reef on  
316 Lake Huron through the Great Lakes Evaporation Network (GLEN) (Blanken et al., 2011;  
317 Spence et al., 2011; Lenters et al., 2013; Spence et al., 2013; Spence et al., 2019). These level-1  
318 eddy covariance data received minimal adjustments, notably the elimination of heat spikes and  
319 a basic visual quality assessment. This dataset was compared with an independent dataset of  
320 Great Lakes' turbulent fluxes developed by Moukomla and Blanken (2017), revealing a "good  
321 statistical agreement" between them, with RMSD ranging from 4.5 to 7 W/m<sup>2</sup> for latent and  
322 sensible heat fluxes (Moukomla and Blanken, 2017).

### 323 3.2 Design of Numerical Experiments

324 We designed numerical experiments in two categories. In category 1, we evaluate the cold  
325 season performance of the NU-WRF/FVCOM two-way coupling (case C1-1) against the NU-  
326 WRF/LISSS 1D lake model (case C1-2). To ensure the objectivity of the comparison, both C1-  
327 1 and C1-2 utilize an identical NU-WRF configuration (except for differences in lake  
328 treatment) as described in Section 2.1, following the optimal NU-WRF configuration for the  
329 study region as determined by Notaro et al. (2021). The comparison of C1-1 and C1-2 aims to



330 examine the overall impact of using a 3D versus a 1D lake model configuration on simulating  
331 lake hydrodynamic conditions and the subsequent impact on the atmospheric state through  
332 lake-ice-atmosphere interactions from November 2014 to March 2015. The initial lake  
333 conditions of November 2014 were obtained from multiple years of FVCOM standalone  
334 simulations driven by Climate Forecast System Reanalysis (CFSR) forcing Xue et al. (2015).

335 In category 2, a set of process-oriented numerical experiments is designed to identify the  
336 impact of various 3D hydrodynamical processes critical to the coupled Great Lakes system.  
337 These processes are either neglected or oversimplified by the NU-WRF/LISSS 1D lake model  
338 while being resolved by the NU-WRF/FVCOM 3D lake model. Case C2-1 (NoIceTransp) is  
339 designed to examine the impact of ice transport associated with currents (Section 5.1). In this  
340 scenario, FVCOM is configured identically to C1-1, except that ice dynamics, ice velocity  
341 fields, and ice pack transport are disabled in FVCOM. Instead, only ice thermal dynamics are  
342 simulated to account for the spatio-temporal evolution of ice thickness distribution through  
343 thermodynamic growth and melting processes (Bitz and Lipscomb, 1999). Consequently, the  
344 ice model is simplified to function as an energy-conserving thermodynamic model, akin to that  
345 used in the 1D lake model.

346 Case C2-2 (NoHeatAdv) analyzes the impact of 3D heat transport associated with lake  
347 circulation. FVCOM is configured identically to C1-1, except that the advective heat transport  
348 associated with current movement is disallowed in C2-2. This is realized by turning off the  
349 advection terms in the temperature equation in FVCOM, which is essentially an advection-  
350 diffusion equation that governs the distribution and evolution of temperature (Section 5.2).  
351 Therefore, the temperature calculation is simplified to imitate the 1D vertical diffusion equation  
352 used in the 1D lake model.

353 Case C2-3 (NoShearProd) aims to assess the influence of 3D currents on calculation of  
354 turbulent mixing, a crucial factor in controlling the heat redistribution and thermal structure in  
355 the lakes. In this case, we exclude the turbulence shear production term that depends on  
356 currents in the turbulent kinetic equation (Section 5.3). In summary, the three cases in category  
357 2 collectively reveal the significant impacts of currents in elements that are not accounted for in  
358 the LISSS 1D lake model, i.e. on ice transport, heat transport, and turbulent mixing intensity,



359 respectively. These experiments are summarized in Table 1.

360 **Table 1.** A summary of the numerical model experiments. The "3D currents" column shows if the  
361 experiment resolves the 3D currents of the Great Lakes. The "Ice transport" column shows if the  
362 experiment resolves the ice transport associated with currents in the Great Lakes. The "Heat advective  
363 transport" column shows if the experiment resolves the 3D heat transport associated with Great Lakes  
364 circulation. The "Shear production in turbulence" column shows if the experiment uses the turbulence  
365 shear production term that depends on currents in the turbulent kinetic equation. The "Lake model"  
366 column shows the lake model used in the experiment.

Experiment	3D currents	Ice transport	Heat advective transport	Shear production in turbulence	Lake model
C1-1 (Lake3D)	Yes	Yes	Yes	Yes	FVCOM
C1-2 (Lake1D)	No	No	No	No	LISSS
C2-1 (NoIceTransp)	Yes	No	Yes	Yes	FVCOM
C2-2 (NoHeatAdv)	Yes	Yes	No	Yes	FVCOM
C2-3 (NoShearProd)	Yes	Yes	Yes	No	FVCOM

367

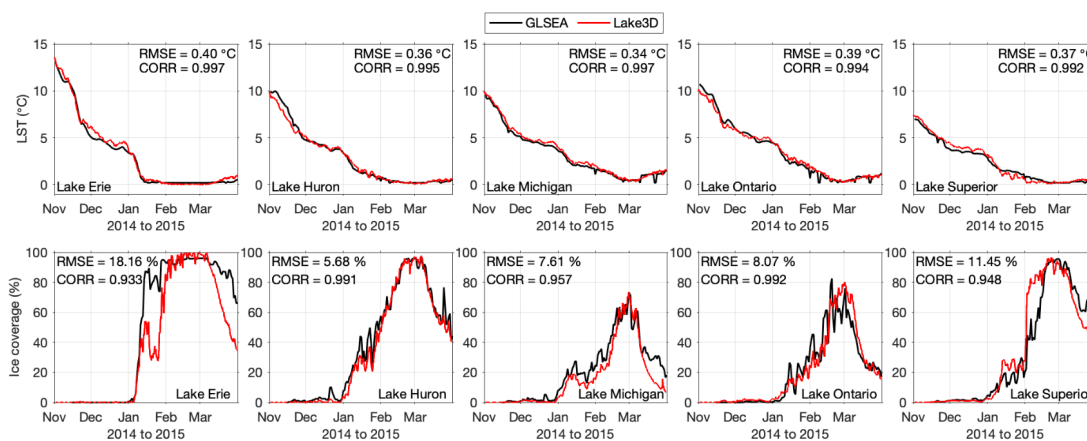
## 368 4 Results

### 369 4.1 Lake Temperature and Ice Coverage

370 The NU-WRF/FVCOM model (case C1-1) accurately captures the seasonal evolution of LSTs  
371 across all of the lakes with lake-mean LST root-mean-square-error (RMSE) less than 0.4°C  
372 (Fig. 2 upper panels). During November, the lakes are in the middle of their cooling period and  
373 the LSTs decrease rapidly, yet at different paces, largely due to variations in the lakes' depth



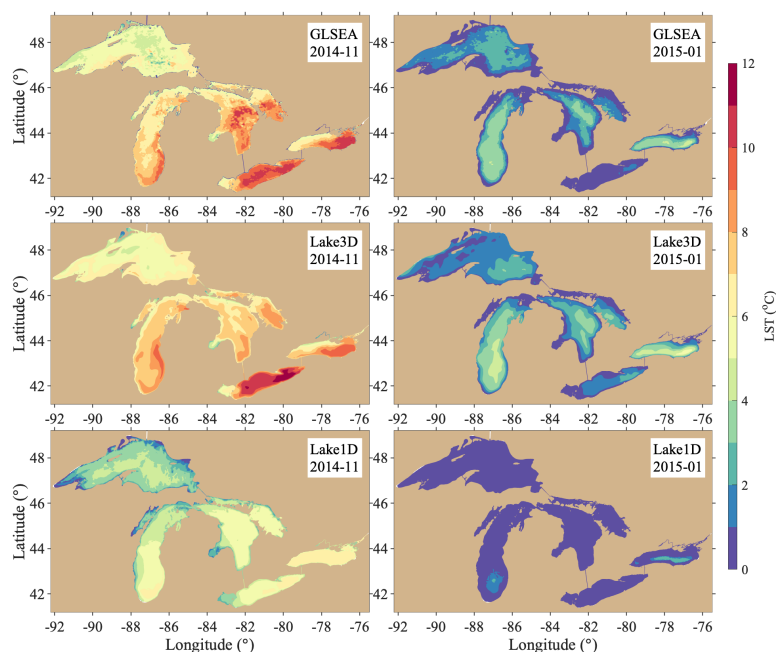
374 and latitude, which leads to strong spatial heterogeneity in LST (Fig. 3, left panels). The  
375 GLSEA data and the 3D lake model closely align in terms of the spatial LST patterns, with  
376 warmer waters of 10-12°C in the central and eastern basins of Lakes Erie and Ontario and 8-  
377 10°C in the southern basins of Lakes Michigan and Huron, while much cooler temperatures are  
378 found across Lake Superior, ranging between 4-6°C. The most notable underestimation of LST  
379 by the 3D lake simulation occurs in the southern basin of Lake Huron, while the model well  
380 captures the LSTs in the northern basin of Lake Huron. Transitioning to January 2015 (Fig. 3,  
381 right panels), at the onset of the ice season, NU-WRF/FVCOM accurately reflects the seasonal  
382 cooling of the lakes, showing a significant reduction in LSTs, while also well delineating the  
383 detailed temperature differences between the colder nearshore and relatively warmer offshore  
384 waters, in good agreement with the observational data. On the other hand, NU-WRF/LISSS  
385 (case C1-2) fails to capture the spatial heterogeneity in LSTs, but also generates a systematic  
386 cold bias of 2-3°C during January across nearly all of the lakes (Fig. 3, bottom panels). Such a  
387 cold bias was persistent in the NU-WRF/LISSS (Lake1D) simulation throughout the cold  
388 season, as detailed in Notaro et al. (2021).



389

390 **Figure 2.** Time series of daily lake-averaged LST (°C, upper panels) and percent ice cover (lower panels)  
391 for the five lakes from GLSEA data (black lines) and NU-WRF/FVCOM 3D lake model simulations (red  
392 lines) during the simulation period of November 2014-March 2015. Both the temporal correlation and  
393 RMSE are reported in each panel.





394

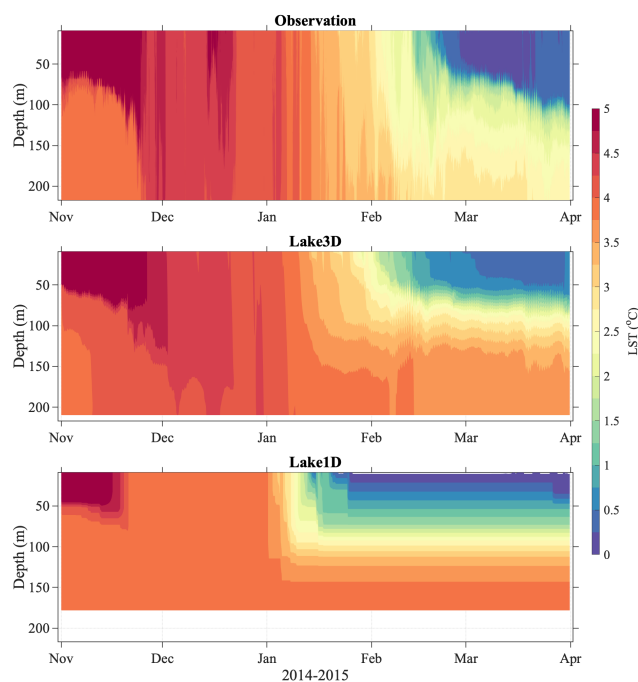
395 **Figure 3.** Spatial patterns of monthly mean LSTs (°C) from GLSEA data (top panels), NU-  
396 WRF/FVCOM 3D lake model simulations (middle panels), and NU-WRF/LISSSS 1D lake model  
397 simulations (bottom panels) for November 2014 (left panels) and January 2015 (right panels).

398 NU-WRF/FVCOM (Lake3D) also demonstrates its skill in capturing the evolution of the  
399 vertical thermal structure within the lake, which is particularly challenging in large and deep  
400 lakes (Bennington et al., 2014; Xue et al., 2017). As exemplified in Fig. 4, the in-situ thermistor  
401 measurement at Spectacle Reef on Lake Huron is located in a deep region with a water depth  
402 greater than 200 meters. The 3D model reproduces the conclusion of the summer stratification  
403 process until the end of November. The following turnover, a seasonal process where the  
404 surface water cools, becomes denser, and sinks—mixing with the warmer water from below—  
405 is also represented in the 3D lake model between December and January. Subsequently, the  
406 winter inverse stratification, where colder water (< 4°C) lies above warmer water due to the fact  
407 that freshwater’s density peaks at 4°C, is captured by the 3D model as it develops from  
408 February onward, although the model shows a stronger winter inverse stratification and earlier  
409 onset than observed. In contrast, NU-WRF/LISSSS falls short of these detailed observations. Not  
410 only does it mispredict the occurrence of turnover and winter stratification much earlier than





411 observed, but it also substantially underestimates the extent of mixing between the surface and  
412 deeper waters. This underestimation results in a flawed representation of excessive surface  
413 cooling and a substantial overestimation of the warming of the deep waters.



414

415 **Figure 4.** Seasonal evolution of daily vertical temperature ( $^{\circ}\text{C}$ ) profiles from the thermistor observations  
416 (top panel), NU-WRF/FVCOM 3D lake model (middle panel), and NU-WRF/LISSS 1D lake model  
417 (bottom panel) at Spectacle Reef in Lake Huron during November 2014-March 2015.

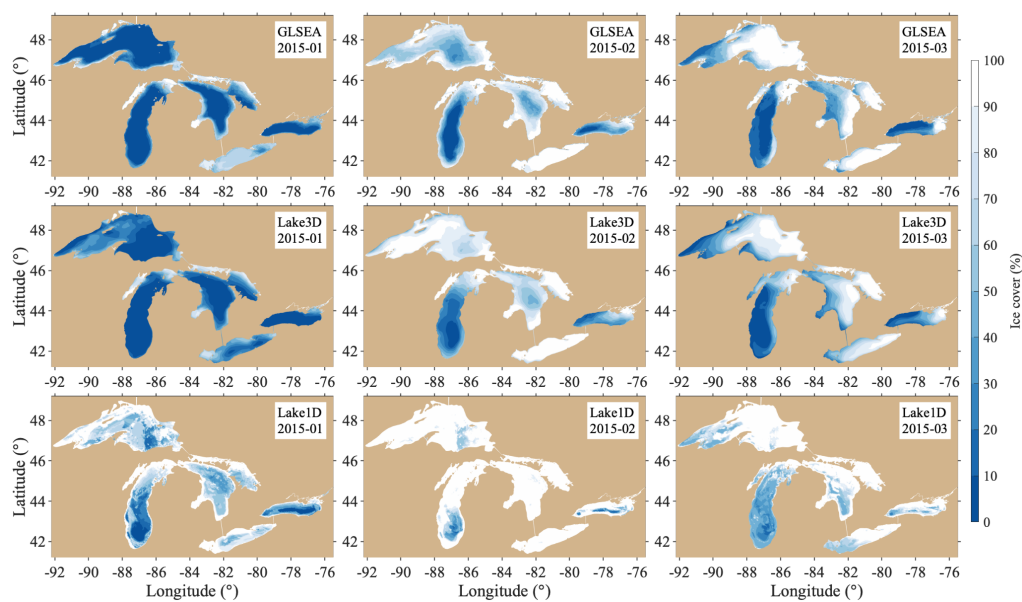
418 Correspondingly, NU-WRF/FVCOM resolves the spatiotemporal evolution of lake ice cover  
419 very well across all of the lakes with RMSE of percent ice cover less than 8% for Lakes Huron,  
420 Michigan, and Ontario and 11% and 18% for Lakes Superior and Erie, respectively (Fig. 2  
421 lower panels). The 3D lake model and GLSEA data exhibit similar seasonal trends both in  
422 timing and magnitude, with ice cover typically starting to rapidly increase in January, peaking  
423 in February and early March, and declining thereafter (Fig. 2). Lake Erie shows the earliest and  
424 sharpest increase in ice cover, peaking near 100% in early February and throughout mid-March,  
425 indicative of its shallower depth and weaker thermal inertia. Lakes Huron and Superior show a



426 persistent increase in ice cover through February, with peak coverage of >90% occurring at the  
427 beginning of March. Lakes Michigan and Ontario exhibit more gradual increases and lower  
428 peaks in ice cover. The model appears to capture the general seasonal trends of the GLSEA  
429 data with high fidelity, although some discrepancies are evident, particularly over Lakes Erie  
430 and Superior (Fig. 2).

431 NU-WRF/FVCOM performs reasonably well in mirroring the general spatial patterns of lake  
432 ice cover (Fig. 5, top and middle panels). For January, the GLSEA data shows a pronounced ice  
433 formation in the nearshore regions across the lakes, with the greatest ice concentration visible  
434 along the coastlines and very limited ice cover in offshore waters. The model captures this  
435 nearshore ice development quite well, although it suggests less ice cover in the offshore areas,  
436 particularly over Lake Erie. In February, the extent of ice cover varies dramatically across the  
437 lakes, including nearly full ice cover on Lake Erie and significant ice-free areas on Lake  
438 Ontario, as well as for Lakes Michigan and Huron, which have distinctly less ice cover in their  
439 southern and central basins, respectively. The model captures this variability very well, while  
440 slightly overestimating the ice cover in the central regions of Lake Superior. For March, the  
441 model successfully replicates the patterns of significant declines in ice cover in the western  
442 sections of the lakes, with much higher ice coverage in the eastern sections of the lakes.

443 On the other hand, NU-WRF/LISSS (Lake1D) generates excessive ice cover during January,  
444 when both observations and NU-WRF/FVCOM suggested that the majority of the lakes were  
445 ice-free. In February, the excessive ice cover simulated by the NU-WRF/LISSS model persists,  
446 with near 100% ice coverage over all of the lakes, and the model fails to depict the large spatial  
447 variability across the lakes. Such a persistent overestimation of ice cover throughout the cold  
448 season by NU-WRF/LISSS was also reported in Notaro et al. (2021).



449

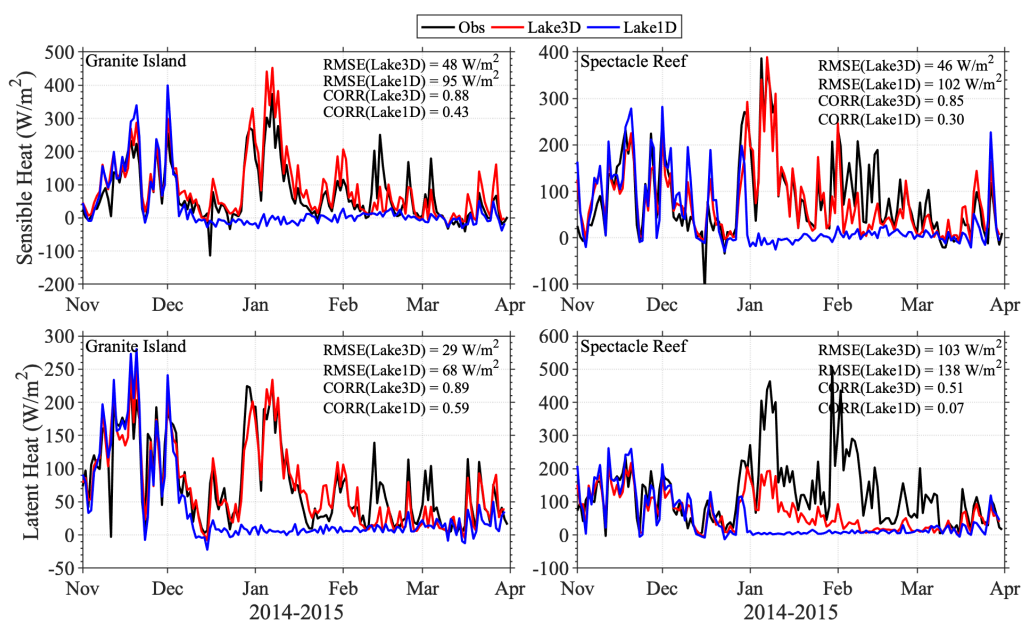
450 **Figure 5.** Spatial patterns of mean percent lake ice cover from GLSEA data (top panels), NU-  
451 WRF/FVCOM 3D lake model simulations (middle panels), and NU-WRF/LISSSS 1D lake model  
452 simulations (bottom panels) for January 2015 (first column), February 2015 (second column), and March  
453 2015 (third column).

#### 454 **4.2 Over-lake Latent and Sensible Heat Fluxes**

455 The improved LST and ice simulation by the 3D lake model translates to an improvement in the  
456 simulated over-lake latent and sensible heat fluxes, particularly for the ice-cover season (Fig.  
457 6). The observations for upward latent and sensible heat fluxes from two eddy covariance flux  
458 towers at Granite Island on Lake Superior and Spectacle Reef on Lake Huron are compared  
459 against the simulated fluxes from NU-WRF/FVCOM (Lake3D) and NU-WRF/LISSS  
460 (Lake1D). The two lakes are selected for demonstration as they have the highest ice coverage  
461 during the simulation period. NU-WRF/LISSS reasonably simulates the magnitude and  
462 variability of the heat fluxes from November until mid-December, similar to the observations  
463 and NU-WRF/FVCOM, although with larger biases. However, it grossly underestimates the  
464 fluxes during the ice-cover season (January-March) by simulating a nearly constant near-zero  
465 flux. This is mainly due to the excessive ice cover simulated by the 1D lake model, which  
466 creates a physical barrier for air-lake energy fluxes. Since the 3D lake model more accurately



467 simulates the LST and ice cover, it successfully captures the magnitude and variability of the  
468 heat fluxes, even during the ice-cover season, with RMSEs that are 50% lower than those from  
469 the 1D lake model (Fig. 6). Latent heat in Spectacle Reef is the only exception, where NU-  
470 WRF/FVCOM struggles to capture the magnitude of the upward latent heat flux due to the  
471 overestimated ice cover at the site. However, it still outperforms NU-WRF/LISSS in terms of  
472 capturing the seasonal trend in latent heat fluxes.



473

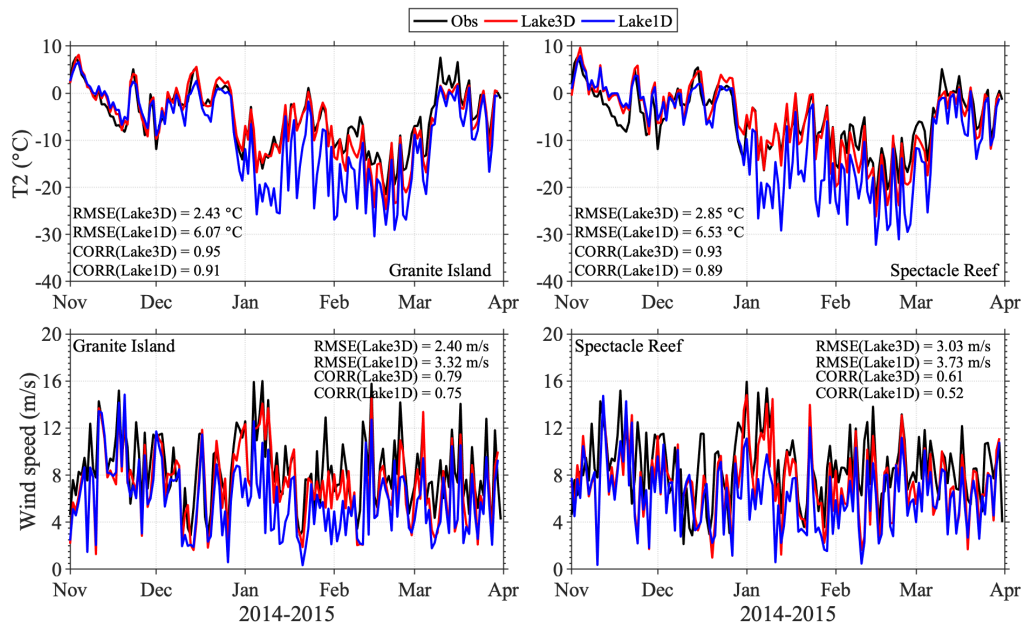
474 **Figure 6.** Time series of daily sensible (upper panels) and latent (lower panels) heat fluxes (W/m<sup>2</sup>) from  
475 GLEN observations (black lines), NU-WRF/FVCOM 3D lake model simulations (red lines), and NU-  
476 WRF/LISSS 1D lake model simulations (blue lines) at Granite Island on Lake Superior (left) and  
477 Spectacle Reef on Lake Huron (right). The RMSE and temporal correlations between the simulations and  
478 GLEN observations are provided in each panel.

### 479 4.3 Over-lake Air Temperature and Wind

480 Along with the improved simulation of the Great Lakes' physical characteristics and surface  
481 heat fluxes, NU-WRF/FVCOM improves the simulated over-lake atmospheric state across the  
482 Great Lakes, including air temperature and wind speed. The cold air temperature biases  
483 produced over the lakes by NU-WRF/LISSS are significantly reduced (Fig. 7) with better



484 simulated, more intense upward heat fluxes in January. This improvement in the simulated air  
485 temperature at the two sites, Granite Island and Spectacle Reef, is clearly evident. Similar to the  
486 fluxes, NU-WRF/LISSS modeled air temperature diverges from the observations in January  
487 and February, with a noticeable cold bias. This cold bias is the result of significant suppression  
488 of the upward heat fluxes during those months in the 1D lake model due to excessive simulated  
489 ice cover. NU-WRF/FVCOM, on the other hand, produces a much warmer and more accurate  
490 over-lake air temperature for January and February due to its reasonable representation of  
491 upward heat fluxes. The simulated wind speed over the lakes is also improved, especially in  
492 January-February (Fig. 7). This advancement is attributed to the refined simulation of surface  
493 roughness (i.e., ice versus water), the water-air temperature gradient, and associated instability  
494 over the lakes due to decreased ice cover. Large wind spikes (16 m/s) in January-February are  
495 more accurately captured by NU-WRF/FVCOM.



496

497 **Figure 7.** Time series of daily air temperature (°C, upper panels) at 2-m height (T2) and wind speed  
498 (m/s, lower panels) from GLEN observations (black lines), NU-WRF/FVCOM 3D lake model  
499 simulations (red lines), and NU-WRF/LISSSS 1D lake model simulations (blue lines) at Granite Island  
500 on Lake Superior and Spectacle Reef on Lake Huron during November 2014-March 2015. The RMSE  
501 and temporal correlations between the simulations and GLEN observations are provided in each panel.



## 502    **5    Discussion**

503    The Great Lakes modeling community has agreed on the pressing need to integrate 3D lake  
504    models instead of conventional 1D lake modeling in the Great Lakes regional climate studies  
505    (Delaney and Milner, 2019). However, no studies have yet detailed the key 3D hydrodynamic  
506    processes that explain the superiority of 3D lake models over 1D lake models, especially  
507    regarding cold season performance and lake-atmosphere interactions. The primary goal of this  
508    study is to identify the crucial processes influencing lake thermal structure and ice cover that  
509    are missed by 1D lake models but effectively captured by 3D lake models, through a series of  
510    process-oriented experiments presented below.

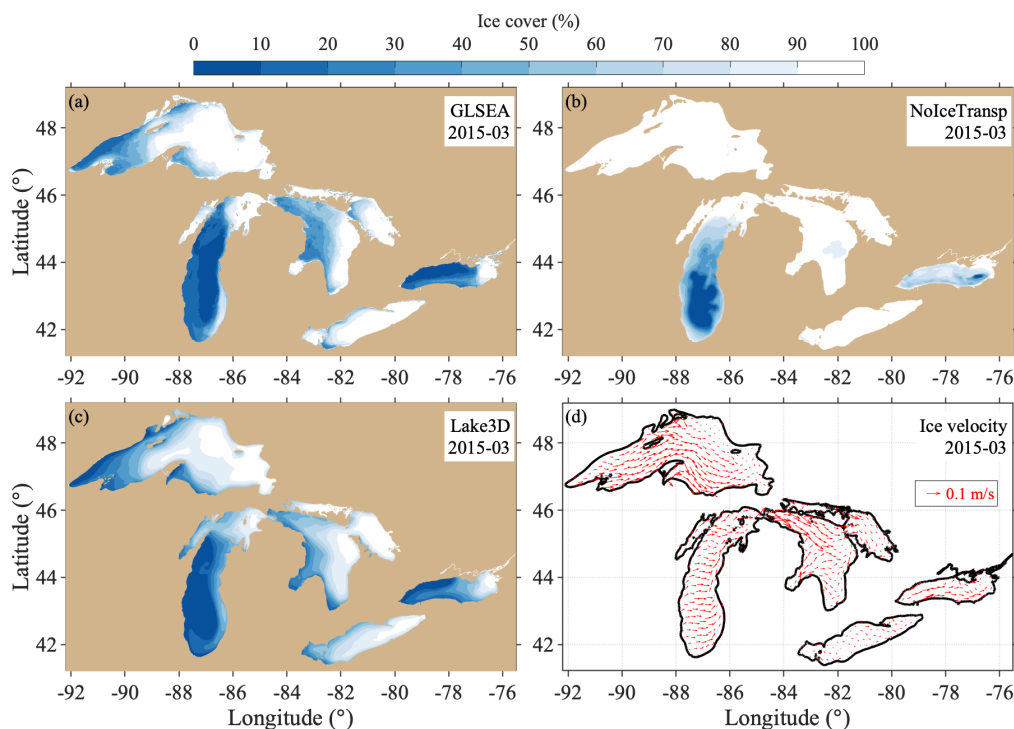
### 511    **5.1    Impact of Ice Movement**

512    The 3D hydrodynamic model, FVCOM, includes an embedded unstructured-grid ice model  
513    capable of resolving several components for atmosphere-ice-water interactions (Gao et al.,  
514    2011). It includes a thermodynamic model that computes the local growth rates of snow and ice  
515    due to vertical conductive, radiative, and turbulent fluxes, aligning with features typically  
516    included in 1D lake models (Bitz and Lipscomb, 1999). More importantly, it features an ice  
517    dynamics model that predicts the ice pack's velocity field based on its material strength; a  
518    transport model that describes the advection of areal concentration, ice volumes, and other state  
519    variables; and a ridging parameterization that facilitates the transfer of ice among thickness  
520    categories (Hunke et al., 2010).

521    Case C2-1 (NoIceTransp) is designed to examine the impact of ice transport on LSTs and  
522    overlying atmospheric conditions, compared to standard case C1-1 (Lake3D). In case C2-1, ice  
523    dynamics, velocity fields, and ice pack transport are disabled in FVCOM. Instead, only ice  
524    thermal dynamics are simulated, as in the 1D lake model. Figure 8 compares cases C1-1  
525    (Lake3D) and C2-1 (NoIceTransp), illustrating their performance in simulating the observed  
526    spatial pattern of ice coverage in March 2015, characterized by open water on the western side  
527    of the Great Lakes and predominant ice cover on the eastern side (Fig. 8a). Utilizing a 3D lake  
528    model that only accounts for ice thermal dynamics results in an overestimation of ice cover,  
529    with near 100% lakewide ice cover in Lakes Superior, Huron, and Erie (Fig. 8b). However,  
530    integrating ice dynamics, including transport influenced by wind and water-ice stress, results in



531 excellent agreement with observations, highlighting the critical role of ice transport in accurate  
532 ice modeling (Fig. 8c). This pattern aligns with the modeled ice velocities, which attribute the  
533 eastward ice cover distribution to dominant eastward ice transport (Fig. 8d). Under cold winter  
534 conditions characterized by strong westerly winds, ice is driven eastward, maintaining open  
535 water in the lake's western part. This facilitates ongoing atmospheric interactions, allowing for  
536 heat release. Neglecting these dynamics leads to unrealistic ice accumulation by diminishing  
537 the influence of wind on surface water movement and mixing. This overaccumulation of ice  
538 cover hampers the efficiency of vertical turbulent mixing, which is essential for maintaining a  
539 warmer surface layer, thereby exacerbating ice formation and accumulation. The incorporation  
540 of ice dynamics into 3D lake models is thus essential for accurately simulating ice distribution,  
541 emphasizing the necessity of resolving ice transport to replicate observed patterns accurately.



542

543 **Figure 8.** Spatial patterns of mean percent lake ice cover from GLSEA data (a), case 2-1 (NoIceTransp)  
544 simulations (b), and case 1-1 (Lake3D) standard simulations (c), along with simulated mean ice  
545 velocities (m/s) during (d) March 2015.





## 546 5.2 Impact of Heat Transport

547 The 3D lake model also resolves the advective transport of heat associated with the simulated  
548 circulation. The advective transport and turbulent mixing of temperature in the 3D lake model  
549 are governed by following equation:

$$550 \quad \frac{\partial T}{\partial t} + u \frac{\partial T}{\partial x} + v \frac{\partial T}{\partial y} + w \frac{\partial T}{\partial z} = \frac{\partial}{\partial z} \left( K_h \frac{\partial T}{\partial z} \right) + F_T \quad (1)$$

551 with the surface heat flux boundary condition:

$$552 \quad \frac{\partial T}{\partial t} = \frac{1}{\rho c_p K_h} [LW(x, y, t) - LH(x, y, t) - SH(x, y, t)] \quad (2)$$

553 where  $T$  is the water temperature and  $u$ ,  $v$ , and  $w$  are the  $x$ ,  $y$ , and  $z$  components of the water  
554 velocity, respectively.  $K_h$  is the vertical thermal diffusivity coefficient and  $F_T$  is the horizontal  
555 diffusion term.  $\rho$  is water density,  $c_p$  is the specific heat capacity of water and  
556  $LW(x, y, t)$ ,  $LH(x, y, t)$ , and  $SH(x, y, t)$  are net longwave radiation, upward latent heat and  
557 sensible heat fluxes varying in space and time, respectively.

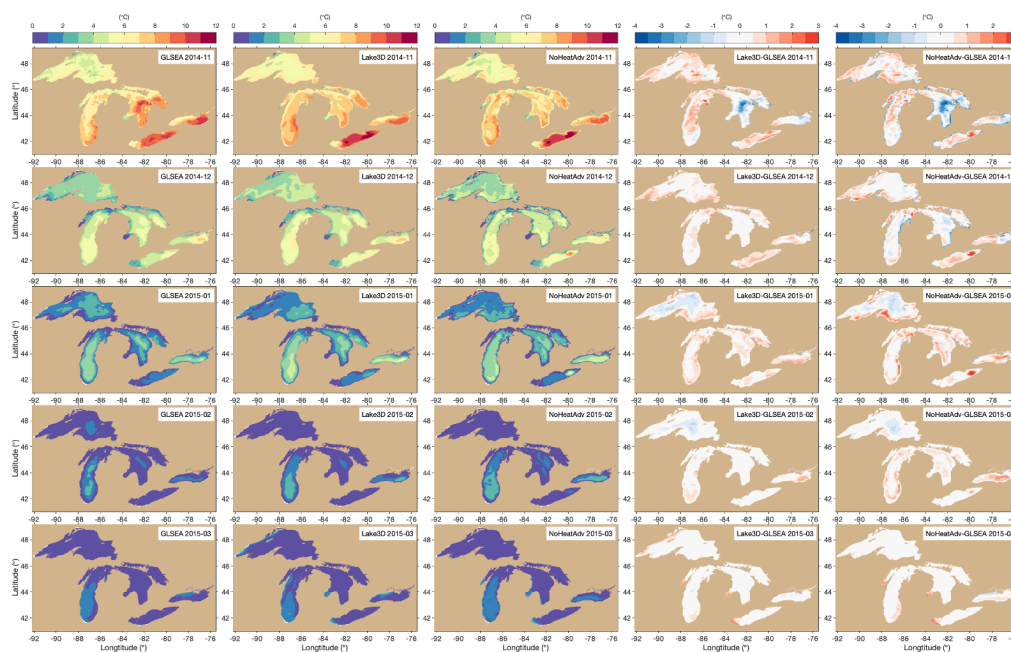
558 Case C2-2 (NoHeatAdv) analyzes the impact of 3D heat transport. In this case, the 3D  
559 temperature advection terms ( $u \frac{\partial T}{\partial x}$ ,  $v \frac{\partial T}{\partial y}$ ,  $w \frac{\partial T}{\partial z}$ ) are turned off.

560 Comparing the standard simulation C1-1 (Lake3D) to case C2-2 (NoHeatAdv), Figure 9  
561 demonstrates that, in the absence of advective heat transport by lake currents, the surface  
562 temperatures can remain consistent with the basic patterns observed in the standard 3D lake  
563 simulation throughout the entire simulation period. The differences in the time series of lake-  
564 wide average LSTs for the five lakes are small, with a maximum difference of 0.4°C between  
565 the two cases. The spatial patterns of LST biases, when compared with GLSEA, are generally  
566 more noticeable, with the most significant positive biases ( $\sim 2^\circ\text{C}$ ) concentrated around the  
567 coastal waters of the Great Lakes and eastern Lake Erie from January to March 2015 and larger  
568 negative biases ( $\sim 3^\circ\text{C}$ ) in the central basin of Lake Huron in November 2014 in the  
569 NoHeatAdv case.





570 In addition, the vertical transport associated with upwelling, resolved by the 3D model, brings  
571 relatively warmer water from deep in the lake to the surface. This vertical transport mechanism  
572 cannot be represented in 1D lake models that only account for vertical diffusion. This can  
573 create significant local-scale differences along the coast, as shown on the western shore of Lake  
574 Superior in March 2015 [Fig. 9, bottom panels. Notice that the GLSEA is not able to well  
575 capture coastal upwelling (Ye et al., 2020)]. This underscores the importance of including  
576 advective heat transport to accurately resolve the redistribution of heat within the lake. The  
577 inclusion of advective dynamics, by facilitating both lateral and vertical redistribution, enables  
578 a more realistic simulation of the complex spatial heat patterns within large lake systems.



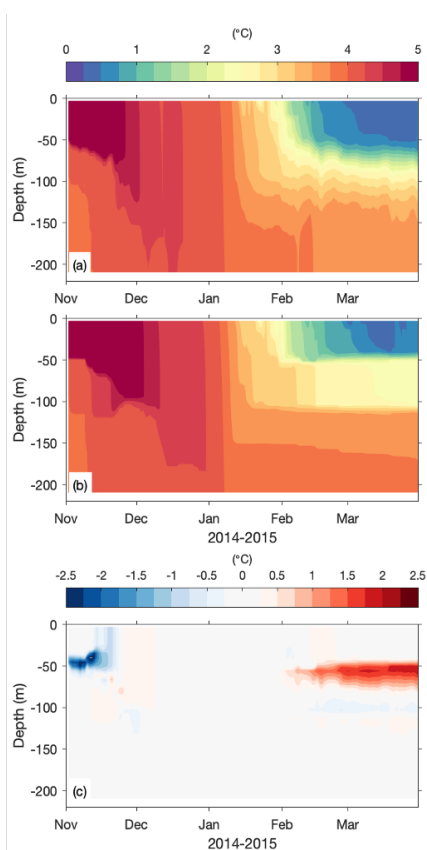
579

580 **Figure 9.** Spatial patterns of mean LSTs ( $^{\circ}\text{C}$ ) from GLSEA data (first column), case C1-1 (Lake3D)  
581 standard simulations (second column), and case C2-2 (NoHeatAdv) simulations (third column) from  
582 November 2014 (top row) to March 2015 (bottom row). Their monthly biases relative to GLSEA data are  
583 presented in the fourth and fifth columns, respectively.

584 Capturing the evolution of the vertical thermal structure within the deep water is particularly  
585 challenging in lake models. As previously shown in Fig. 4, the in-situ thermistor measurement



586 at Spectacle Reef on Lake Huron is located in a deep region with a water depth greater than 200  
587 meters. Case C2-2 (NoHeatAdv) generally reproduced the thermal patterns from case C1-1  
588 (Lake3D) in terms of both timing and intensity of summer stratification, fall turnover, and  
589 winter inverse stratification (Fig. 10a,b). While the comparison shows that the overall thermal  
590 structures are similar in both simulations, there is a noticeable difference within the subsurface  
591 layer, specifically between 50 to 100 meters in depth (Fig. 10c), suggesting that heat advection  
592 might have a more significant impact on temperature distribution in the subsurface layer of the  
593 water column in this case. Without accounting for heat advective transport, there appears to be  
594 artifacts of stepwise vertical thermal gradients in case C2-2.

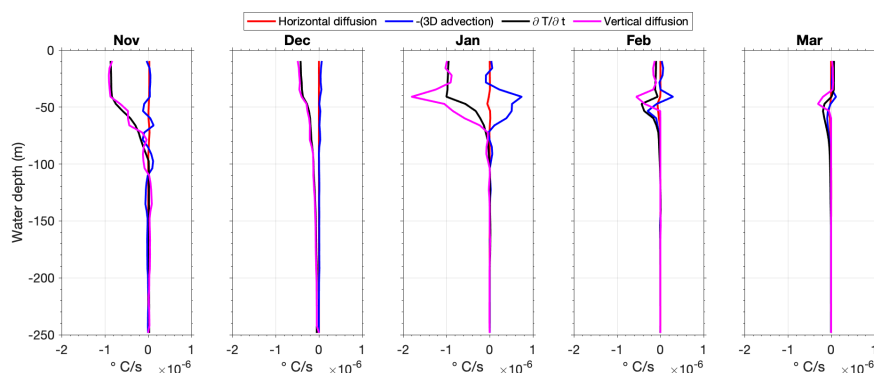


595

596 **Figure 10.** Mean vertical temperature ( $^{\circ}\text{C}$ ) profiles from a): case C1-1 (Lake3D) standard run and b):  
597 case C2-2 (NoHeatAdv) and c): their difference at Spectacle Reef in Lake Huron during November 2014-  
598 March 2015.



599 To gain a deeper understanding of the results, we analyzed the heat balance to identify the  
600 contributions of different physical processes. This analysis involved examining each term in the  
601 temperature governing equation (Eq. 1) that is directly computed in FVCOM over the  
602 simulation period. The temperature change is driven by 3D advective heat transport, horizontal  
603 heat diffusion, and vertical diffusion due to turbulent mixing.



604

605 **Figure 11.** Monthly averaged vertical profile of each term of the temperature equation in the C1-1  
606 (Lake3D) simulation from November 2014 to March 2015, output from location at Spectacle Reef in  
607 Lake Huron. The temperature change rate ( $\frac{\partial T}{\partial t}$ ) is determined by 3D advection (blue), horizontal diffusion  
608 (red), and vertical diffusion (purple).

609 The analysis revealed the relative impact of physical processes on thermal changes during the  
610 winter months (Fig. 11). Significant cooling and decreasing temperatures were observed within  
611 the upper 100 meters of the water column, as indicated by the negative temperature change over  
612 time ( $\frac{\partial T}{\partial t}$ ) in this zone. In contrast, the water below 100 meters in depth remained largely  
613 unchanged and stable in temperature. In November and December, vertical turbulent mixing  
614 processes primarily controlled the cooling rate in the upper 100 meters, during which surface  
615 heat fluxes served as net losses from the lake along with vigorous turbulent mixing in the lake.  
616 Advection played a much less important role in temperature changes during this period.  
617 However, starting in January, 3D advection played an important role in redistributing heat in  
618 the 25-100 meter layer, offsetting some of the cooling induced by surface heat loss through  
619 mixing. In February and March 2015, advection proved to be significant at the lower boundary



620 of the surface mixed layer. These observations explain the larger temperature difference in the  
621 subsurface layer between cases C1-1 (Lake3D) and C2-2 (NoHeatAdv) (Fig. 10), highlighting  
622 the evolving balance between vertical diffusion and advection in controlling the epilimnetic  
623 heat budget and temperature changes in large lakes during the cold season.

### 624 5.3 Impact of Vertical Mixing

625 The analysis above (Fig. 11) highlights the dominant factor, vertical turbulent mixing, in  
626 determining seasonal lake temperature change. Note that we have already discussed the  
627 importance of ice transport associated with currents as well as the impact of advective heat  
628 transport. To understand the mechanism responsible for the differing performance between the  
629 1D and 3D lake models in simulating vertical mixing, we examine how vertical turbulent  
630 mixing is calculated in these two types of models. The intensity of vertical mixing in both  
631 models is represented by vertical eddy diffusivity, which is determined by turbulent kinetic  
632 energy ( $q^2$ ). In the 3D hydrodynamic lake model, a sophisticated 3D turbulence closure model  
633 is used, in which a prognostic equation predicts the change rate of  $q^2$  based on its advection,  
634 and its turbulence production, including both shear-induced production ( $P_s$ ) and buoyancy-  
635 induced production ( $P_b$ ), and its dissipation rate ( $\epsilon$ ), as well as its diffusion. This equation is  
636 complemented by either a separate prognostic equation for dissipation rate (k- $\epsilon$ ; Launder and  
637 Spalding, 1974) or a diagnostic equation for turbulent mixing length (Meller and Yamada,  
638 1982).

639 The equation governing the evolution of turbulent kinetic energy ( $q^2$ ) is

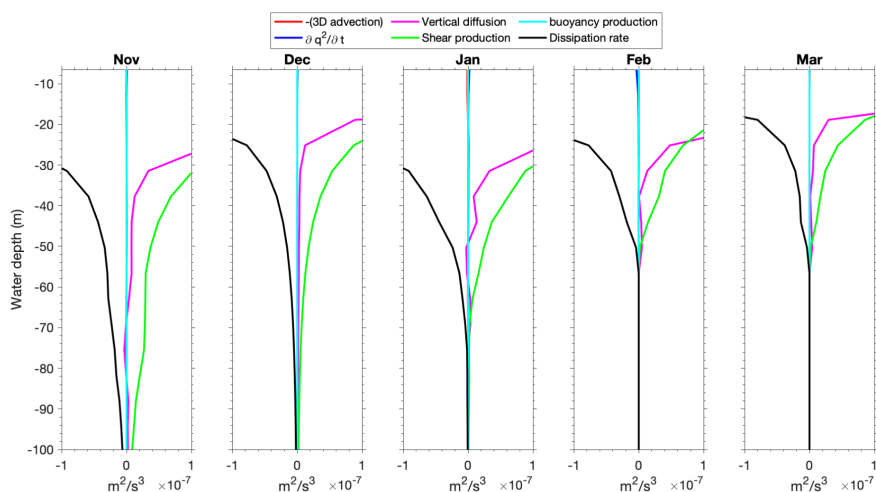
$$640 \quad \frac{\partial q^2}{\partial t} + u \frac{\partial q^2}{\partial x} + v \frac{\partial q^2}{\partial y} + w \frac{\partial q^2}{\partial z} = P_s + P_b - \epsilon + \frac{\partial}{\partial z} \left( K_q \frac{\partial q^2}{\partial z} \right) + F_q \quad (3)$$

641 where  $q^2 = (\langle u'^2 \rangle + \langle v'^2 \rangle + \langle w'^2 \rangle)/2$ , with  $u', v', w'$  represent the fluctuating components of  
642 velocity in the  $x, y, z$  directions, respectively. The  $\langle \rangle$  denotes averaging over time or space to  
643 obtain the mean. Shear production is often approximated as  $P_s = K_m \left( \left( \frac{\partial u}{\partial z} \right)^2 + \left( \frac{\partial v}{\partial z} \right)^2 \right)$ , where  
644  $K_m$  is the vertical eddy viscosity coefficient. Buoyancy production is computed as  $P_b =$   
645  $-\frac{g}{\rho_0} K_h \frac{\partial \rho}{\partial z}$ , where  $g$  is acceleration due to gravity.  $\rho_0$  is reference density of the fluid (e.g.,



646 ocean water or air).  $K_h$  is thermal diffusivity,  $\frac{\partial \rho}{\partial z}$  is vertical gradient of density, indicating  
647 stratification. The turbulent kinetic energy dissipation rate is represented as  $\epsilon = q^3 / Bl$ , where  
648  $l$  is the turbulence length scale and  $B$  is an empirical constant.  $K_{m,h,q} = qlS_{m,h,q}$ , where  $S_{m,h,q}$   
649 are stability functions for  $K_{m,h,q}$ , respectively.  $K_q$  is the vertical diffusivity coefficient for  
650 turbulent kinetic energy and  $F_q$  is horizontal diffusion of the turbulent kinetic energy .

651 Figure 12 reveals that in the Great Lakes, shear production—induced by the vertical gradient of  
652 horizontal velocity in the water column—is the primary driver of subsurface turbulent mixing.  
653 Conversely, buoyancy production plays a secondary role, being at least one order of magnitude  
654 smaller than shear production in the first 50 meters of depth. This underscores the importance  
655 of including accurate current simulation when estimating the vertical turbulent mixing, which is  
656 crucial for accurately simulating heat exchange in the water column and ultimately determining  
657 the lake's thermal structure and ice formation.

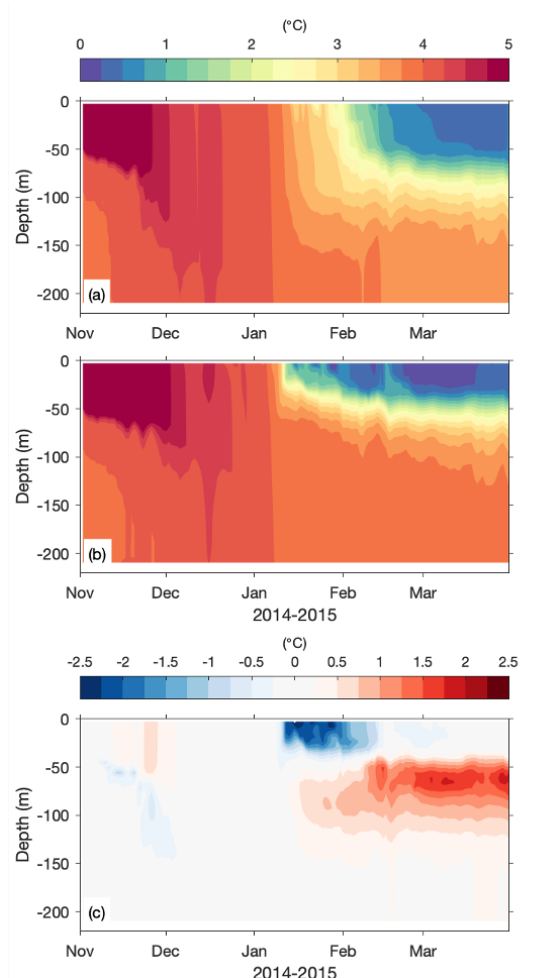


658

659 **Figure 12.** Monthly averaged vertical profile of each term of the turbulence kinetic equation in the C1-1  
660 (Lake3D) simulation from November 2014 to March 2015, at Spectacle Reef on Lake Huron. The change  
661 rate of turbulent kinetic energy (blue) is based on the 3D advection (red), and the turbulence production,  
662 including both shear-induced production (green) and buoyancy-induced production (cyan), the  
663 dissipation rate (black), and vertical diffusion (purple).



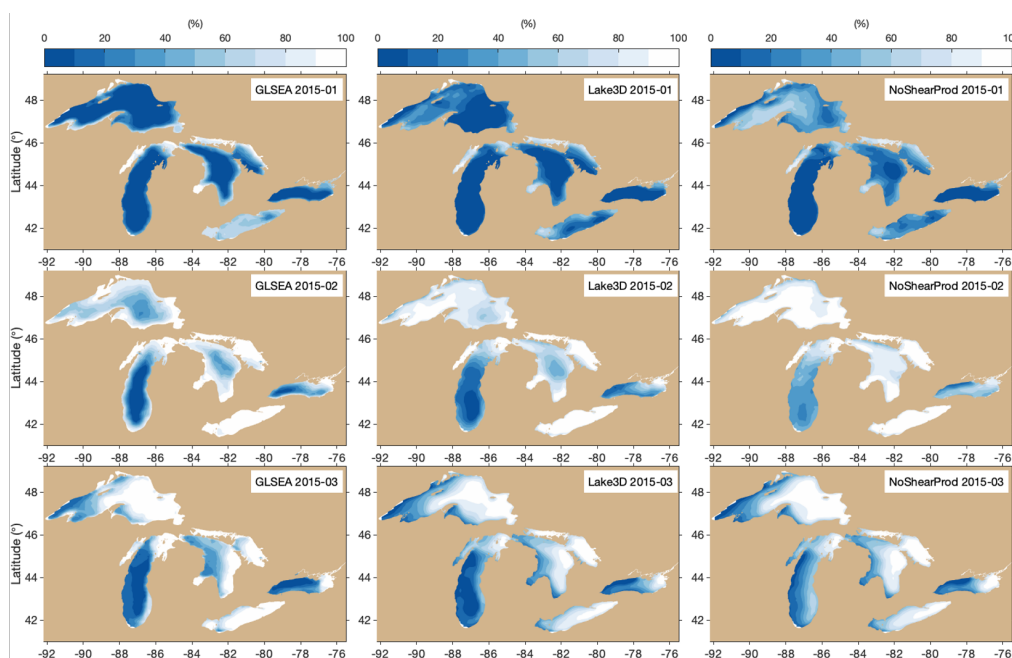
664 Figure 13 compares the vertical temperature profiles between the standard simulation C1-1  
665 (Lake3D) and case C2-3 (NoShearProd). The NoShearProd case shows much stronger  
666 stratification, particularly from January to March. The absence of shear production leads to  
667 significantly reduced turbulent mixing and limiting heat exchange between surface and deeper  
668 waters, which results in a much colder surface layer (0-40 m) in January and much warmer  
669 deep waters (50-150 m) in February and March compared to the standard run. Consequently,  
670 the colder surface water temperature favors ice formation, leading to overestimated ice cover in  
671 the NoShearProd case compared to the standard simulation and observations, particularly in  
672 January and February (Fig. 14).



673



674 **Figure 13.** Mean vertical temperature ( $^{\circ}\text{C}$ ) profiles from a): case C1-1 (Lake3D) standard run and b):  
675 case C2-3 (NoShearProd) and c): their difference at Spectacle Reef on Lake Huron during November  
676 2014-March 2015.



677

678 **Figure 14.** Spatial patterns of mean percent lake ice cover from GLSEA data (first column), case C1-1  
679 (Lake3D; second column) and case 2-3 (NoShearProd; third column) for January 2015 (first row),  
680 February 2015 (second row), and March 2015 (third row).

681 LISSS, as true of other 1D lake models, was originally designed for small and shallow inland  
682 lakes and was not designed to resolve water currents (Subin et al., 2012; Notaro et al., 2021).  
683 Some other 1D lake models (Stepanenko and Lykossov, 2005; Stepanenko et al., 2011) employ  
684 a crude representation of average flow fields. Therefore, 1D lake models rely on empirical or  
685 semi-empirical relationships to estimate how wind stress affects the lake's turbulence and  
686 mixing without explicitly resolving 3D velocity fields. These thermal diffusion-based models  
687 often employ a latitude-dependent Ekman decay, accompanied by an empirical modification  
688 factor, to estimate a lumped eddy diffusivity coefficient as an approximation for surface wind-  
689 induced mixing (Xiao et al., 2016). Thus, the lack of accurate simulation of turbulent mixing



690 processes makes the 1D model of limited capacity in accurately simulating the Great Lakes'  
691 thermal structure.

## 692 **6 Summary and Conclusion**

693 In summary, a two-way coupled NU-WRF/FVCOM model (CLIAv1) has been developed  
694 toward the next generation of a regional climate model for the Great Lakes Basin for accurate  
695 representations of lake–ice–atmosphere interactions. NU-WRF/FVCOM significantly improved  
696 on the performance of NU-WRF coupled with an optimized 1D lake model, and accurately  
697 reproduced the physical characteristics of the Great Lakes (e.g., LST, ice cover, and thermal  
698 structure). This led to further improvements in simulated over-lake atmospheric conditions  
699 (e.g., air temperature, wind, latent and sensible heat) through two-way lake-atmosphere  
700 interactions.

701 While 1D column lake models have been widely used in the simulations of inland lakes  
702 worldwide, small inland lakes and the Great Lakes exhibit fundamental differences in their  
703 physical characteristics, such as size and depth, which in turn influence their mixing behaviors,  
704 thermal structures, and circulation patterns. Inland lakes, generally much smaller (with a typical  
705 average area of 1-10 kilometers) and much shallower (with a typical average depth of ~10m),  
706 respond more rapidly to atmospheric conditions. This leads to a fairly uniform horizontal  
707 pattern and a simpler mixing process in response to surface wind, due to their shallow depth  
708 and small thermal inertia. Therefore, 1D column lake models serve as an appropriate and  
709 efficient tool for simulating inland lake processes, particularly when the lake depth is shallower  
710 than 20 meters. In contrast, the vast size (e.g., Lake Superior alone covers about 82,100 square  
711 kilometers) and significant depth (e.g., the average depth of Lake Superior is 147 m, with a  
712 maximum depth of 400 m) of the Great Lakes result in complex hydrodynamic and thermal  
713 dynamics. This complexity causes the Great Lakes to exhibit many sea-like characteristics.

714 This study has highlighted key physical processes that differentiate the large, deep Great Lakes  
715 from small, shallow inland lakes, and how these processes impact lake simulations.  
716 Specifically, we identified that ice dynamics, particularly ice transport, are vital in the Great  
717 Lakes, influencing ice cover formation and heat exchange between the lake and the atmosphere.





718 Secondly, we show that advective heat transport, facilitates both lateral and vertical  
719 redistribution, enables a more realistic simulation of the complex spatial temperature patterns,  
720 particularly the predominance of advective heat transport in the subsurface layers. Thirdly, we  
721 identified the critical role of resolving shear production in turbulent mixing in the Great Lakes,  
722 which is the most influential factor that determines heat transfer and, subsequently, lake  
723 thermal structure. Ice transport, heat transfer, and shear production in turbulence mixing are  
724 fundamentally linked to the 3D lake currents, which are missing or crudely represented in 1D  
725 lake models. Our findings underscore that circulation currents are pivotal in the physical  
726 limnology of the Great Lakes. Given the ongoing impact of climate change on these aquatic  
727 systems (Zhong et al., 2016; Woolway et al., 2021; Cannon et al., 2024), accurately  
728 incorporating 3D lake dynamics becomes crucial for projecting future thermal structures and  
729 ecosystem effects.

730 Lastly, we acknowledge that there are multiple ways to tune the 1D lake column model or build  
731 an accurate empirical relationship between atmospheric conditions and the strength of mixing  
732 to improve 1D model simulations. However, the major challenge with this approach is that any  
733 empirical or simplified physical relationship carries significant risks of not holding in the  
734 future, especially in the context of climate change. While it may work well to calibrate the  
735 model based on a substantial amount of validation data, this approach has a much larger risk  
736 and lacks reliability if the model is used for climate projections where conditions change  
737 significantly. Therefore, we advocate for the complete integration of 3D hydrodynamic lake  
738 models in a two-way coupled fashion to project future changes in large freshwater systems.  
739 This method ensures that projections are based on physical processes, reducing the risk  
740 associated with empirical relationships and increasing the model's reliability for future climate  
741 scenarios.

#### 742 **Code and data availability**

743 The source codes of CLIAv1 with the two-way coupled FVCOM and NU-WRF used in this  
744 study are available at <https://doi.org/10.5281/zenodo.12746348> (Huang, 2024a) and  
745 <https://doi.org/10.5281/zenodo.12746306> (Huang, 2024b) respectively. The GLSEA data were  
746 obtained from the NOAA Coastwatch website (<https://coastwatch.glerl.noaa.gov/glsea/doc/>)



747 (GLSEA, 2023). The GLEN data were from the Lake Superior Watershed Partnership website  
748 (<https://superiorwatersheds.org/GLEN/>), with data compilation and publication provided by  
749 LimnoTech under Award/Contract 10042-400759 from the International Joint Commission  
750 (IJC) through a subcontract with the Great Lakes Observing System (GLOS).

#### 751 **Author contributions**

752 PX conceived the study. PX and CH developed the model code. PX designed the experiments.  
753 PX, MN, XZ, CH, MBK, and CZ conducted the analyses. PX, MN, MBK, and CZ wrote the  
754 original manuscript. All others contributed to revising the manuscript. All authors have read  
755 and agreed to the published version of the manuscript.

#### 756 **Competing interests**

757 The authors declare that they have no conflict of interest.

#### 758 **Acknowledgments**

759 This is the Contribution No. 121 of the Great Lakes Research Center at Michigan  
760 Technological University. The study was funded by NASA's Modeling, Analysis, and  
761 Prediction Program (Grant 80NSSC17K0287 and Grant 80NSSC17K0291). Hydrodynamic  
762 modeling was also partly supported by the U.S. Department of Energy, Office of Science, under  
763 award number DE-SC0024446. The statements, findings, conclusions, and recommendations of  
764 authors expressed herein do not necessarily state or reflect those of the United States  
765 Government or any agency thereof.

766



## 767 References

- 768 Assel, A. A. (1990). An ice-cover climatology for Lake Erie and Lake Superior for the winter  
769 seasons 1897–1898 to 1982–1983. *International Journal of Climatology*, 10(7), 731-  
770 748.
- 771 Assel, R. A. (2005). Classification of Annual Great Lakes Ice Cycles: Winters of 1973-2002.  
772 *Journal of Climate*, 18, 4895. Retrieved from  
773 <https://ui.adsabs.harvard.edu/abs/2005JCLI...18.4895A>
- 774 Assel, R. A., Norton, D. C., & Cronk, K. C. (2002). A Great Lakes ice cover digital data set for  
775 winters 1973-2000.
- 776 Assel, R. A., Wang, J., Clites, A. H., & Bai, X. (2013). Analysis of Great Lakes ice cover  
777 climatology: Winters 2006-2011.
- 778 Ballentine, R. J., Stamm, A. J., Chermack, E. E., Byrd, G. P., & Schleede, D. (1998).  
779 Mesoscale model simulation of the 4–5 January 1995 lake-effect snowstorm. *Weather*  
780 *and Forecasting*, 13(4), 893-920.
- 781 Bennington, V., Notaro, M., & Holman, K. D. (2014). Improving Climate Sensitivity of Deep  
782 Lakes within a Regional Climate Model and Its Impact on Simulated Climate. *Journal*  
783 *of Climate*, 27(8), 2886-2911. doi:<https://doi.org/10.1175/jcli-d-13-00110.1>
- 784 Bitz, C. M., & Lipscomb, W. H. (1999). An energy-conserving thermodynamic model of sea  
785 ice. *Journal of Geophysical Research: Oceans*, 104(C7), 15669-15677.
- 786 Blanken, P. D., Spence, C., Hedstrom, N., & Lenters, J. D. (2011). Evaporation from Lake  
787 Superior: 1. Physical controls and processes. *J. Great Lakes Res.*, 37, 707-716.
- 788 Botts, L., & Krushelnicki, B. (1987). *The Great Lakes. An Environmental Atlas and Resource*  
789 *Book*: ERIC.
- 790 Briley, L. J., Rood, R. B., & Notaro, M. (2021). Large lakes in climate models: A Great Lakes  
791 case study on the usability of CMIP5. *Journal of Great Lakes Research*, 47(2), 405-  
792 418. doi:<https://doi.org/10.1016/j.jglr.2021.01.010>
- 793 Brown, L. C., & Duguay, C. R. (2010). The response and role of ice cover in lake-climate  
794 interactions. *Progress in Physical Geography*, 34(5), 671-704.
- 795 Bullock, O. R., Alapaty, K., Herwehe, J. A., Mallard, M. S., Otte, T. L., Gilliam, R. C., &  
796 Nolte, C. G. (2014). An observation-based investigation of nudging in WRF for  
797 downscaling surface climate information to 12-km grid spacing. *Journal of Applied*  
798 *Meteorology and Climatology*, 53(1), 20-33.
- 799 Cannon, D., Wang, J., Fujisaki-Manome, A., Kessler, J., Ruberg, S., & Constant, S. (2024).  
800 Investigating Multidecadal Trends in Ice Cover and Subsurface Temperatures in the  
801 Laurentian Great Lakes Using a Coupled Hydrodynamic–Ice Model. *Journal of*  
802 *Climate*, 37(4), 1249-1276. doi:<https://doi.org/10.1175/JCLI-D-23-0092.1>
- 803 Changnon, S. A., Jr., & Jones, D. M. A. (1972). Review of the influences of the Great Lakes on  
804 weather. *Water Resources Research*, 8.
- 805 Chen, C., Beardsley, R., Cowles, G., Qi, J., Lai, Z., Gao, G., . . . Ge, J. (2012). *An unstructured-*  
806 *grid, finite-volume community ocean model: FVCOM user manual*: Sea Grant College  
807 Program, Massachusetts Institute of Technology Cambridge . . .
- 808 Chin, M., Rood, R. B., Lin, S. J., Müller, J. F., & Thompson, A. M. (2000). Atmospheric sulfur  
809 cycle simulated in the global model GOCART: Model description and global  
810 properties. *Journal of Geophysical Research: Atmospheres*, 105(D20), 24671-24687.
- 811 Chuang, H.-Y., & Sousounis, P. J. (2003). The impact of the prevailing synoptic situation on  
812 the lake-aggregate effect. *Monthly Weather Review*, 131(5), 990-1010.



- 813 Collins, W. D., Rasch, P. J., Boville, B. A., Hack, J. J., McCaa, J. R., Williamson, D. L., . . .  
814 Lin, S.-J. (2004). Description of the NCAR community atmosphere model (CAM 3.0).  
815 *NCAR Tech. Note NCAR/TN-464+ STR*, 226, 1326-1334.
- 816 Colucci, S. J. (1976). winter cyclone frequencies over the eastern United States and adjacent  
817 western Atlantic, 1964–1973: Student paper—First place winner of The Father James  
818 B. Macelwane Annual Award in Meteorology, announced at the Annual Meeting of the  
819 AMS, Philadelphia, Pa., 21 January 1976. *Bulletin of the American Meteorological*  
820 *Society*, 57(5), 548-553.
- 821 Craig, A., Valcke, S., & Coquart, L. (2017). Development and performance of a new version of  
822 the OASIS coupler, OASIS3-MCT\_3. 0. *Geoscientific Model Development*, 10(9),  
823 3297-3308.
- 824 Crossman, E. J., & Cudmore, B. C. (1998). Biodiversity of the fishes of the Laurentian Great  
825 Lakes: a great lakes fishery commission project. *Italian Journal of Zoology*, 65(S1),  
826 357-361.
- 827 Delaney, F., & Milner, G. (2019). *The State of Climate Modeling in the Great Lakes Basin - A*  
828 *Synthesis in Support of a Workshop held on June 27, 2019 in Arr Arbor, MI*. Retrieved  
829 from [https://climateconnections.ca/app/uploads/2020/05/The-State-of-Climate-](https://climateconnections.ca/app/uploads/2020/05/The-State-of-Climate-Modeling-in-the-Great-Lakes-Basin_Sept132019.pdf)  
830 [Modeling-in-the-Great-Lakes-Basin\\_Sept132019.pdf](https://climateconnections.ca/app/uploads/2020/05/The-State-of-Climate-Modeling-in-the-Great-Lakes-Basin_Sept132019.pdf)
- 831 Eichenlaub, V. L. (1978). Weather and climate of the Great Lakes region [USA]. *University of*  
832 *Notre Dame Press*.
- 833 Environmental Protection Agency (EPA). (2014). State of the Great Lakes 2011. *EPA 950-R-*  
834 *13-002*. Retrieved from [https://archive.epa.gov/solec/web/pdf/sogl-2011-technical-](https://archive.epa.gov/solec/web/pdf/sogl-2011-technical-report-en.pdf)  
835 [report-en.pdf](https://archive.epa.gov/solec/web/pdf/sogl-2011-technical-report-en.pdf)
- 836 Gao, G., Chen, C., Qi, J., & Beardsley, R. C. (2011). An unstructured-grid, finite-volume sea  
837 ice model: Development, validation, and application. *Journal of Geophysical Research:*  
838 *Oceans*, 116(C8).
- 839 Gao, Y., Fu, J. S., Drake, J., Liu, Y., & Lamarque, J.-F. (2012). Projected changes of extreme  
840 weather events in the eastern United States based on a high resolution climate modeling  
841 system. *Environmental Research Letters*, 7(4), 044025.
- 842 Gerbush, M. R., Kristovich, D. A., & Laird, N. F. (2008). Mesoscale boundary layer and heat  
843 flux variations over pack ice-covered Lake Erie. *Journal of Applied Meteorology and*  
844 *Climatology*, 47(2), 668-682.
- 845 Giorgi, F., & Gutowski Jr., W. J. (2015). Regional Dynamical Downscaling and the CORDEX  
846 Initiative. *Annual Review of Environment and Resources*, 40(1), 467-490.  
847 doi:10.1146/annurev-environ-102014-021217
- 848 Goudsmit, G. H., Burchard, H., Peeters, F., & Wüest, A. (2002). Application of k- $\epsilon$  turbulence  
849 models to enclosed basins: The role of internal seiches. *Journal of Geophysical*  
850 *Research: Oceans*, 107(C12), 23-21-23-13.
- 851 Gu, H., Jin, J., Wu, Y., Ek, M. B., & Subin, Z. M. (2015). Calibration and validation of lake  
852 surface temperature simulations with the coupled WRF-lake model. *Climatic Change*,  
853 129, 471-483.
- 854 Hanrahan, J., Langlois, J., Cornell, L., Huang, H., Winter, J. M., Clemins, P. J., . . . Bruyère, C.  
855 (2021). Examining the Impacts of Great Lakes Temperature Perturbations on Simulated  
856 Precipitation in the Northeastern United States. *Journal of Applied Meteorology and*  
857 *Climatology*, 60(7), 935-949.
- 858 Holman, K. D., Gronewold, A., Notaro, M., & Zarrin, A. (2012). Improving historical  
859 precipitation estimates over the Lake Superior basin. *Geophysical Research Letters*,  
860 39(3).



- 861 Hostetler, S. W., & Bartlein, P. J. (1990). Simulation of lake evaporation with application to  
862 modeling lake level variations of Harney-Malheur Lake, Oregon. *Water Resources*  
863 *Research*, 26(10), 2603-2612. doi:10.1029/WR026i010p02603
- 864 Huang, C. (2024a). Lake model code for the manuscript "On the Importance of Coupling a 3D  
865 Hydrodynamic Model with a Regional Climate Model in Simulating the Great Lakes  
866 Winter Climate" [Software]. Zenodo. doi:<https://doi.org/10.5281/zenodo.12746348>
- 867 Huang, C. (2024b). NU-WRF (v11) code for the manuscript "On the Importance of Coupling a  
868 3D Hydrodynamic Model with a Regional Climate Model in Simulating the Great  
869 Lakes Winter Climate" [Software]. Zenodo.  
870 doi:<https://doi.org/10.5281/zenodo.12746306>
- 871 Hunke, E. C., & Dukowicz, J. K. (1997). An elastic–viscous–plastic model for sea ice  
872 dynamics. *Journal of Physical Oceanography*, 27(9), 1849-1867.
- 873 Hunke, E. C., Lipscomb, W. H., Turner, A. K., Jeffery, N., & Elliott, S. (2010). Cice: the los  
874 alamos sea ice model documentation and software user's manual version 4.1 la-cc-06-  
875 012. *T-3 Fluid Dynamics Group, Los Alamos National Laboratory*, 675, 500.
- 876 Hutson, A., Fujisaki-Manome, A., & Lofgren, B. (2024). Testing the Sensitivity of a WRF-  
877 based Great Lakes Regional Climate Model to Cumulus Parameterization and Spectral  
878 Nudging. *Journal of Hydrometeorology*. doi:<https://doi.org/10.1175/JHM-D-22-0234.1>
- 879 Kain, J. S. (2004). The Kain–Fritsch convective parameterization: an update. *Journal of*  
880 *Applied Meteorology*, 43(1), 170-181.
- 881 Kain, J. S., & Fritsch, J. M. (1990). A one-dimensional entraining/detraining plume model and  
882 its application in convective parameterization. *Journal of Atmospheric Sciences*,  
883 47(23), 2784-2802.
- 884 Kayastha, M. B., Huang, C., Wang, J., Pringle, W. J., Chakraborty, T., Yang, Z., . . . Xue, P.  
885 (2023). Insights on Simulating Summer Warming of the Great Lakes: Understanding  
886 the Behavior of a Newly Developed Coupled Lake-Atmosphere Modeling System.  
887 *Journal of Advances in Modeling Earth Systems*, 15(7), e2023MS003620.
- 888 Kristovich, D. A. R., & Laird, N. F. (1998). Observations of Widespread Lake-Effect  
889 Cloudiness: Influences of Lake Surface Temperature and Upwind Conditions. *Weather*  
890 *and Forecasting*, 13(3), 811-821. doi:10.1175/1520-  
891 0434(1998)013<0811:Oowlec>2.0.Co;2
- 892 Kumar, S. V., Peters-Lidard, C. D., Tian, Y., Houser, P. R., Geiger, J., Olden, S., . . . Dirmeyer,  
893 P. (2006). Land information system: An interoperable framework for high resolution  
894 land surface modeling. *Environmental Modelling & Software*, 21(10), 1402-1415.
- 895 Lam, D. C., & Schertzer, W. M. (1999). *Potential climate change effects on Great Lakes*  
896 *hydrodynamics and water quality*: ASCE Publications.
- 897 Lenters, J., Anderton, J., Blanken, P., Spence, C., & Suyker, A. (2013). Assessing the Impacts  
898 of Climate Variability and Change on Great Lakes Evaporation. 2011 Project Reports.  
899 D. Brown, D. Bidwell, and L. Briley, eds. Available from the Great Lakes Integrated  
900 Sciences and Assessments (GLISA) Center. In.
- 901 Lofgren, B. M. (2014). Simulation of atmospheric and lake conditions in the Laurentian Great  
902 Lakes region using the Coupled Hydrosphere-Atmosphere Research Model (CHARM).
- 903 Mallard, M., Nolte, C., Spero, T., Bullock, O., Alapaty, K., Herwehe, J., . . . Bowden, J. (2015).  
904 Technical challenges and solutions in representing lakes when using WRF in  
905 downscaling applications. *Geoscientific Model Development*, 8(4), 1085-1096.
- 906 Mallard, M. S., Nolte, C. G., Bullock, O. R., Spero, T. L., & Gula, J. (2014). Using a coupled  
907 lake model with WRF for dynamical downscaling. *Journal of Geophysical Research:*  
908 *Atmospheres*, 119(12), 7193-7208.



- 909 Martynov, A., Sushama, L., & Laprise, R. (2010). Simulation of temperate freezing lakes by  
910 one-dimensional lake models: performance assessment for interactive coupling with  
911 regional climate models. *Boreal environment research*, 15(2), 143.
- 912 Martynov, A., Sushama, L., Laprise, R., Winger, K., & Dugas, B. (2012). Interactive lakes in  
913 the Canadian Regional Climate Model, version 5: the role of lakes in the regional  
914 climate of North America. *Tellus A: Dynamic Meteorology and Oceanography*, 64(1),  
915 16226.
- 916 Matsui, T., Iguchi, T., Li, X., Han, M., Tao, W.-K., Petersen, W., . . . Kummerow, C. D. (2013).  
917 GPM satellite simulator over ground validation sites. *Bulletin of the American  
918 Meteorological Society*, 94(11), 1653-1660.
- 919 Matsui, T., Santanello, J., Shi, J., Tao, W. K., Wu, D., Peters-Lidard, C., . . . Sekiguchi, M.  
920 (2014). Introducing multisensor satellite radiance-based evaluation for regional Earth  
921 system modeling. *Journal of Geophysical Research: Atmospheres*, 119(13), 8450-8475.
- 922 Mellor, G. L., & Yamada, T. (1982). Development of a turbulence closure model for  
923 geophysical fluid problems. *Reviews of Geophysics*, 20(4), 851-875.  
924 doi:<https://doi.org/10.1029/RG020i004p00851>
- 925 Minallah, S., & Steiner, A. L. (2021). The effects of lake representation on the regional  
926 hydroclimate in the ECMWF reanalyses. *Monthly Weather Review*, 149(6), 1747-1766.
- 927 Mironov, D., Heise, E., Kourzeneva, E., Ritter, B., Schneider, N., & Terzhevik, A. (2010).  
928 Implementation of the lake parameterisation scheme FLake into the numerical weather  
929 prediction model COSMO.
- 930 Mitchell, K. (2005). The community Noah land-surface model (LSM). *User's Guide Public  
931 Release Version*, 2(1).
- 932 Mlawer, E. J., Taubman, S. J., Brown, P. D., Iacono, M. J., & Clough, S. A. (1997). Radiative  
933 transfer for inhomogeneous atmospheres: RRTM, a validated correlated-k model for  
934 the longwave. *Journal of Geophysical Research: Atmospheres*, 102(D14), 16663-  
935 16682. doi:<https://doi.org/10.1029/97JD00237>
- 936 Mooney, P., Mulligan, F., & Fealy, R. (2013). Evaluation of the sensitivity of the weather  
937 research and forecasting model to parameterization schemes for regional climates of  
938 Europe over the period 1990–95. *Journal of Climate*, 26(3), 1002-1017.
- 939 Morrison, H., Thompson, G., & Tatarskii, V. (2009). Impact of cloud microphysics on the  
940 development of trailing stratiform precipitation in a simulated squall line: Comparison  
941 of one-and two-moment schemes. *Monthly Weather Review*, 137(3), 991-1007.
- 942 Moukomla, S., & Blanken, P. D. (2017). The estimation of the North American Great Lakes  
943 turbulent fluxes using satellite remote sensing and MERRA reanalysis data. *Remote  
944 Sens.*, 9, 141. doi:<https://doi.org/10.3390/rs9020141>
- 945 Nakanish, M. (2001). Improvement of the Mellor–Yamada turbulence closure model based on  
946 large-eddy simulation data. *Boundary-Layer Meteorology*, 99, 349-378.
- 947 Nakanishi, M., & Niino, H. (2006). An improved Mellor–Yamada level-3 model: Its numerical  
948 stability and application to a regional prediction of advection fog. *Boundary-Layer  
949 Meteorology*, 119, 397-407.
- 950 Nakanishi, M., & Niino, H. (2009). Development of an improved turbulence closure model for  
951 the atmospheric boundary layer. *Journal of the Meteorological Society of Japan. Ser.  
952 II*, 87(5), 895-912.
- 953 Niziol, T. A., Snyder, W. R., & Waldstreicher, J. S. (1995). Winter weather forecasting  
954 throughout the eastern United States. Part IV: Lake effect snow. *Weather and  
955 Forecasting*, 10(1), 61-77.
- 956 NOAA Great Lakes Surface Environmental Analysis (GLSEA). (2023). Sea Surface





- 957 Temperature (SST) from Great Lakes Surface Environmental Analysis (GLSEA)  
958 [Dataset]. [Available from:  
959 [https://coastwatch.glerl.noaa.gov/erddap/files/GLSEA\\_GCS/](https://coastwatch.glerl.noaa.gov/erddap/files/GLSEA_GCS/), accessed 2023/11/09]  
960 Notaro, M., Bennington, V., & Vavrus, S. (2015). Dynamically Downscaled Projections of  
961 Lake-Effect Snow in the Great Lakes Basin\*,+. *Journal of Climate*, 28, 1661-1684.  
962 doi:<https://doi.org/10.1175/JCLI-D-14-00467.1>  
963 Notaro, M., Holman, K., Zarrin, A., Fluck, E., Vavrus, S., & Bennington, V. (2013a). Influence  
964 of the Laurentian Great Lakes on Regional Climate. *Journal of Climate*, 26(3), 789-  
965 804. doi:<https://doi.org/10.1175/jcli-d-12-00140.1>  
966 Notaro, M., Zarrin, A., Vavrus, S., & Bennington, V. (2013b). Simulation of Heavy Lake-  
967 Effect Snowstorms across the Great Lakes Basin by RegCM4: Synoptic Climatology  
968 and Variability\*,+. *Monthly Weather Review*, 141(6), 1990-2014. doi:10.1175/mwr-d-  
969 11-00369.1  
970 Notaro, M., Zhong, Y., Xue, P., Peters-Lidard, C., Cruz, C., Kemp, E., . . . Vavrus, S. J. (2021).  
971 Cold Season Performance of the NU-WRF Regional Climate Model in the Great Lakes  
972 Region. *Journal of Hydrometeorology*, 22(9), 2423-2454.  
973 doi:<https://doi.org/10.1175/JHM-D-21-0025.1>  
974 Oleson, K., Lawrence, D., & Bonan, G. B. (2013). Technical description of version 4.5 of the  
975 Community Land Model (CLM). Near Tech. Note NCAR/TN-503+STR. National  
976 Center for Atmospheric Research, Boulder.  
977 Perroud, M., Goyette, S., Martynov, A., Beniston, M., & Annevillec, O. (2009). Simulation of  
978 multiannual thermal profiles in deep Lake Geneva: A comparison of one-dimensional  
979 lake models. *Limnology and Oceanography*, 54(5), 1574-1594.  
980 Peters-Lidard, C. D., Houser, P. R., Tian, Y., Kumar, S. V., Geiger, J., Olden, S., . . . Adams, J.  
981 (2007). High-performance Earth system modeling with NASA/GSFC's Land  
982 Information System. *Innovations in Systems and Software Engineering*, 3, 157-165.  
983 Peters-Lidard, C. D., Kemp, E. M., Matsui, T., Santanello Jr, J. A., Kumar, S. V., Jacob, J. P., .  
984 . . Hou, A. (2015). Integrated modeling of aerosol, cloud, precipitation and land  
985 processes at satellite-resolved scales. *Environmental Modelling & Software*, 67, 149-  
986 159.  
987 Petterssen, S., & Calabrese, P. A. (1959). On some weather influences due to warming of the  
988 air by the Great Lakes in winter. *Journal of Atmospheric Sciences*, 16(6), 646-652.  
989 Rau, E., Vaccaro, L., Riseng, C., & Read, J. G. (2020). The Dynamic Great Lakes Economy  
990 Employment Trends from 2009 to 2018. Retrieved from  
991 <https://repository.library.noaa.gov/view/noaa/38612>  
992 Riley, M. J., & Stefan, H. G. (1988). MINLAKE: A dynamic lake water quality simulation  
993 model. *Ecological Modelling*, 43(3-4), 155-182.  
994 Schwab, D. J., Leshkevich, G. A., & Muhr, G. C. (1999). Automated Mapping of Surface  
995 Water Temperature in the Great Lakes. *Journal of Great Lakes Research*, 25(3), 468-  
996 481. doi:[https://doi.org/10.1016/S0380-1330\(99\)70755-0](https://doi.org/10.1016/S0380-1330(99)70755-0)  
997 Scott, R. W., & Huff, F. A. (1996). Impacts of the Great Lakes on Regional Climate  
998 Conditions. *Journal of Great Lakes Research*, 22(4), 845-863.  
999 doi:[https://doi.org/10.1016/S0380-1330\(96\)71006-7](https://doi.org/10.1016/S0380-1330(96)71006-7)  
1000 Sharma, A., Hamlet, A. F., Fernando, H. J. S., Catlett, C. E., Horton, D. E., Kotamarthi, V. R., .  
1001 . . Wuebbles, D. J. (2018). The Need for an Integrated Land-Lake-Atmosphere  
1002 Modeling System, Exemplified by North America's Great Lakes Region. *Earth's*  
1003 *Future*, 6(10), 1366-1379. doi:<https://doi.org/10.1029/2018ef000870>  
1004 Shi, J., Matsui, T., Tao, W. K., Tan, Q., Peters-Lidard, C., Chin, M., . . . Kemp, E. (2014).



- 1005 Implementation of an aerosol–cloud–microphysics–radiation coupling into the NASA  
1006 unified WRF: Simulation results for the 6–7 August 2006 AMMA special observing  
1007 period. *Quarterly Journal of the Royal Meteorological Society*, 140(684), 2158–2175.  
1008 Shi, Q., & Xue, P. (2019). Impact of Lake Surface Temperature Variations on Lake Effect  
1009 Snow Over the Great Lakes Region. *Journal of Geophysical Research: Atmospheres*,  
1010 124(23), 12553–12567. doi:10.1029/2019jd031261  
1011 Smagorinsky, J. (1963). General Circulation Experiments with the Primitive Equations: I. The  
1012 Basic Experiment *Monthly Weather Review*, 91(3), 99–164. doi:10.1175/1520-  
1013 0493(1963)091<0099:Gcewtp>2.3.Co;2  
1014 Song, Y., Semazzi, F. H., Xie, L., & Ogallo, L. J. (2004). A coupled regional climate model for  
1015 the Lake Victoria basin of East Africa. *International Journal of Climatology*, 24(1), 57-  
1016 75.  
1017 Spence, C., Blanken, P. D., Hedstrom, N., Fortin, V., & Wilson, H. (2011). Evaporation from  
1018 Lake Superior: 2. Spatial distribution and variability. *J. Great Lakes Res.*, 37, 717–724.  
1019 doi:<https://doi.org/10.1016/j.jglr.2011.08.013>  
1020 Spence, C., Blanken, P. D., Lenters, J. D., & Hedstrom, N. (2013). The importance of spring  
1021 and autumn atmospheric conditions for the evaporation regime of Lake Superior. *J.*  
1022 *Hydrometeor.*, 14, 1647–1658. doi:<https://doi.org/10.1175/JHM-D-12-0170.1>  
1023 Spence, C., Hedstrom, N., Blanken, P., Lenters, J., & Cutrell, G. (2019). Great Lakes  
1024 Evaporation Network (GLEN) data. Great Lakes Observing System (GLOS). In.  
1025 Spero, T. L., Nolte, C. G., Bowden, J. H., Mallard, M. S., & Herwehe, J. A. (2016). The impact  
1026 of incongruous lake temperatures on regional climate extremes downscaled from the  
1027 CMIP5 archive using the WRF model. *Journal of Climate*, 29(2), 839–853.  
1028 Stepanenko, V., & Lykossov, V. (2005). Numerical modeling of heat and moisture transfer  
1029 processes in a system lake-soil. *Russ. Meteorol. Hydrol.*, 3, 95–104.  
1030 Stepanenko, V., Machul'Skaya, E., Glagolev, M., & Lykossov, V. (2011). Numerical modeling  
1031 of methane emissions from lakes in the permafrost zone. *Izvestiya, Atmospheric and*  
1032 *Oceanic Physics*, 47, 252–264.  
1033 Stepanenko, V. M., Goyette, S., Martynov, A., Perroud, M., Fang, X., & Mironov, D. (2010).  
1034 First steps of a lake model intercomparison project: LakeMIP. *Boreal environment*  
1035 *research*, 15(2), 191.  
1036 Subin, Z. M., Riley, W. J., & Mironov, D. (2012). An improved lake model for climate  
1037 simulations: Model structure, evaluation, and sensitivity analyses in CESM1. *Journal*  
1038 *of Advances in Modeling Earth Systems*, 4(1).  
1039 doi:<https://doi.org/10.1029/2011MS000072>  
1040 Sun, L., Liang, X.-Z., & Xia, M. (2020). Developing the Coupled CWRP-FVCOM Modeling  
1041 System to Understand and Predict Atmosphere-Watershed Interactions Over the Great  
1042 Lakes Region. *Journal of Advances in Modeling Earth Systems*, 12(12),  
1043 e2020MS002319. doi:<https://doi.org/10.1029/2020MS002319>  
1044 Todorovich, P. (2009). America's emerging megaregions and implications for a national growth  
1045 strategy. *International Journal of Public Sector Management*, 22(3), 221–234.  
1046 Vaccaro, L., & Read, J. (2011). *Vital to Our Nation's Economy: Great Lakes Jobs*. Retrieved  
1047 from [https://www.michiganseagrant.org/wp-content/uploads/2018/10/11-203-Great-](https://www.michiganseagrant.org/wp-content/uploads/2018/10/11-203-Great-Lakes-Jobs-report.pdf)  
1048 [Lakes-Jobs-report.pdf](https://www.michiganseagrant.org/wp-content/uploads/2018/10/11-203-Great-Lakes-Jobs-report.pdf)  
1049 Valcke, S., Redler, R., Budich, R., Valcke, S., & Redler, R. (2012). The oasis coupler. *Earth*  
1050 *System Modelling-Volume 3: Coupling Software and Strategies*, 23–32.  
1051 Wang, J., Bai, X., Hu, H., Clites, A., Colton, M., & Lofgren, B. (2012). Temporal and Spatial  
1052 Variability of Great Lakes Ice Cover, 1973–2010\*. *Journal of Climate*, 25(4), 1318–





- 1053 1329. doi:<https://doi.org/10.1175/2011jcli4066.1>  
1054 Wang, J., Xue, P., Pringle, W., Yang, Z., & Qian, Y. (2022). Impacts of Lake Surface  
1055 Temperature on the Summer Climate Over the Great Lakes Region. *Journal of*  
1056 *Geophysical Research: Atmospheres*, 127(11), e2021JD036231.  
1057 doi:<https://doi.org/10.1029/2021JD036231>  
1058 Woolway, R. I., Anderson, E. J., & Albergel, C. (2021). Rapidly expanding lake heatwaves  
1059 under climate change. *Environmental Research Letters*, 16(9), 094013.  
1060 Xiao, C., Lofgren, B. M., Wang, J., & Chu, P. Y. (2016). Improving the lake scheme within a  
1061 coupled WRF-lake model in the Laurentian Great Lakes. *Journal of Advances in*  
1062 *Modeling Earth Systems*, 8(4), 1969-1985. doi:<https://doi.org/10.1002/2016MS000717>  
1063 Xue, P., Pal, J. S., Ye, X., Lenters, J. D., Huang, C., & Chu, P. Y. (2017). Improving the  
1064 Simulation of Large Lakes in Regional Climate Modeling: Two-Way Lake–  
1065 Atmosphere Coupling with a 3D Hydrodynamic Model of the Great Lakes. *Journal of*  
1066 *Climate*, 30(5), 1605-1627. doi:<https://doi.org/10.1175/jcli-d-16-0225.1>  
1067 Xue, P., Schwab, D. J., & Hu, S. (2015). An investigation of the thermal response to  
1068 meteorological forcing in a hydrodynamic model of Lake Superior. *Journal of*  
1069 *Geophysical Research: Oceans*, 120(7), 5233-5253.  
1070 doi:<https://doi.org/10.1002/2015JC010740>  
1071 Xue, P., Ye, X., Pal, J. S., Chu, P. Y., Kayastha, M. B., & Huang, C. (2022). Climate  
1072 projections over the Great Lakes Region: using two-way coupling of a regional climate  
1073 model with a 3-D lake model. *Geosci. Model Dev.*, 15(11), 4425-4446.  
1074 doi:10.5194/gmd-15-4425-2022  
1075 Ye, X., Chu, P. Y., Anderson, E. J., Huang, C., Lang, G. A., & Xue, P. (2020). Improved  
1076 thermal structure simulation and optimized sampling strategy for Lake Erie using a data  
1077 assimilative model. *Journal of Great Lakes Research*, 46(1), 144-158.  
1078 doi:<https://doi.org/10.1016/j.jglr.2019.10.018>  
1079 Yeates, P., & Imberger, J. (2003). Pseudo two-dimensional simulations of internal and  
1080 boundary fluxes in stratified lakes and reservoirs. *International Journal of River Basin*  
1081 *Management*, 1(4), 297-319.  
1082 Zhong, Y., Notaro, M., Vavrus, S. J., & Foster, M. J. (2016). Recent accelerated warming of the  
1083 Laurentian Great Lakes: Physical drivers. *Limnology and Oceanography*, 61(5), 1762-  
1084 1786. doi:<https://doi.org/10.1002/lno.10331>

1085